Nanostructures for Chemical Sensors
A Specific Targeted Research Project of FP6

STRP 505895-1

NanoChemSens

Nanostructures for Chemical Sensors

Priority 3 – NMP

Nanotechnologies and Nanosciences

Publishable Final Activity Report

Due date of deliverable: 14.4.07

Actual submission date: 10.10.07

Project start date: 01.03.2004 Project duration: 36 months

Project coordinator: Heinrich-Heine-Universität Düsseldorf

Project co-funded by the European Commission within the Sixth Framework Programme (2002-2006)		
Dissimination level		
PU	Public	

Table of Contents

1 Introduction

The project “Nanostructures for Chemical Sensors” (NanoChemSens) has identified and advanced appropriate surface science tools and nanotechnology for the development of chemical sensing nanodevices. It was the intention of the project to understand the nanoscale phenomena that control sensor nanostructures and functionalised surfaces. NanoChemSens project partners include the University of Copenhagen, Düsseldorf, University College London, University of Aix-Marseille III, University of Padova, Charles University of Prague, CRI University of Bourgogne, Roskilde University Center, PBI-Dansensor A/S, FORCE Technology, VEGATEC, BERNT MEASURING TECHNOLOGY and Danish Micro Engineering A/S.

The first objective of the project is the development of suitable techniques for atomically controlled fabrication of nanostructured sensors (“Processing of sensor nanostructures and functionalised surfaces”). The second objective is to extend our understanding of length scales, the degree of complexity associated with nanostructure behaviour, processes of relevance for chemical sensors and sensor/ molecule interactions on functionalised surfaces having sensitive structures of nanosize dimension (“Fundamental studies and new concepts on sensor nanostructures and functionalised surfaces”). The third objective is to test the sensor performance of model nanostructures and to develop potential routes from fundamental studies to sensor development for nanostructured sensors (“Control of the properties of processed sensor nanostructures and functionalised surfaces”).

Conventional electronic conductance sensors with semiconducting metal oxides rely on materials and structures of high complexity of the sensing layer with respect to bulk, surfaces, grain boundaries, and interfaces with the contacts and the substrate. Because of the strong influence of the morphology of the sensing layer, a distinction is commonly made between compact layers, for which the interaction with gases takes place only at the geometric surface, and porous layers. In the context of the NanoChemSens project, it seems more suitable to distinguish between the following basic types of sensors

- heterojunctions,
- metal-oxide-metal tunnel junctions.
- pn junctions,
- epitaxial and thin layers,
- nanorod assemblies, and
- functional organic molecules and ionophores for mass-sensitive devices

and to use model systems for experimental studies towards the above-mentioned objectives of the project.

2 Metal-oxide-metal tunnel junctions and heterojunctions

We have chosen single-crystals of rutile-phase titanium dioxide (TiO_2), terminated by the thermodynamically most stable (110) surface; rutile-TiO_2 is one of the best investigated oxide and hence is regarded as a “prototypical” n-conducting transition metal oxide.[1] Figure 1 indicates schematically a TiO_2 crystal with (a) a nanosized contact of Pt, Pd or Au, (b) catalytically active MoO_x nanostructures and (c) with an ultrathin layer of a mixed Cr-Ti-oxide (CTO).

[1] U. Diebold, *Surf. Sci. Rep*. **48** (2003) 53

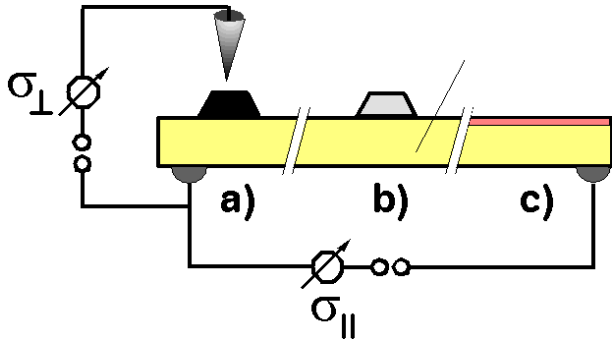

Figure 1. Various nanostructures over TiO_2. a) Pt Schottky diode; b) catalytically active MoO_x; c) mixed Cr-Ti-oxide films. $\sigma_{\perp}$ and $\sigma_{||}$ denote the conductance measured perpendicularly and parallel to the surface, respectively.

Schottky diodes, revealing sensing properties, are known for silicon (PdAg/thin SiO_2/Si for H_2 sensing and Pd/SiC)[2] and also for oxide seminconducting materials (e.g. Pt/ZnO for CO sensing)[3]. Recently, Somorjai and Xiaozhong Ji has constructed a nanoscale Schottky diode, based upon a 150-nm-thick layer of TiO_2 and a 5-nm-thick platinum film, which is used to measure a continuous flow of hot electrons generated by catalytic surface reactions.[4] Au has found interest because of its high catalytic activity for low-temperature CO oxidation when Au particles become very small and are distributed over oxide surfaces. A corresponding effect can be expected for gas sensing devices since the sensing reactions involve catalytic steps. Similarly, oxidic nanostructures may lead to a significant enhancement of sensor responses of semiconducting devices. CTO is a useful material for reduction of water cross-sensitivity[5], used for NH_3 sensing. Also ultrathin MoO_x films are of interest as metal oxide, providing potentially an active surface for sensors.

Figure 1 a may also serve as a sketch of an arrangement in which a tungsten tip, attached to the *z*-piezo tube of a scanning tunneling microscope (STM), is used to "contact" a single Pt crystal on a TiO_2(110) surface. By decreasing the cluster-tip spacing from a start value z_0 (typically at I = 0,6 nA), through the voltage applied to the *z*-piezo, one can form an intimate electrical connection. The value z_0 is the distance previously adjusted in the constant-current operation mode of the STM. By taking current-voltage curves one can be study the effect of oxygen dosing to such a *nanoscopic Schottky-diode* arrangement.[6] As a prerequisite several techniqual issues of the experiment, developed over the course of the project, have to be refined. Firstly, the preparation technique for Pt clusters over TiO_2(110) surfaces was optimized in order to create nanocrystals of a suitable lateral spacing between each other. We used the so-called "seeding and growing" technique.[7] Small amounts of Pt are deposited on a clean TiO_2(110) surface, followed by an anneal at 1000 K, thus forming very small nucleation centres for subsequent Pt that is evaporated at a high temperature (1000 K) in uhv. This procedure circumvents the problem of surfaces that are covered with a great number of smaller clusters at a high density. Besides the optimization of the Pt growth technique, also instrumental improvements were achieved. We replaced the tunneling current amplifier in our instrument, providing only a constant gain, by a multiple-gain amplifier. It has a number of selectable gains and can thus be operated under normal STM conditions (currents are typically in the range of 0.1 to 1 nA) but can also be used to measure currents after contact formation (typically above 100 nA) with sufficient resolution and dynamics. We explore the use of the following software-controlled procedure; after positioning the W tip over the Pt cluster, the feedbacks stabilizes the

---

[2] Hughes et al. *Appl. Phys. A*. **62** (1987) 1074

[3] Kang et al., *Appl. Phys. A*. **80** (2005) 259

[4] X. Ji, A. Zuppero, J. M. Gidwani, and G. A. Somorjai, *Nano Lett*. **5** (2005) 753

[5] P.T. Moseley, D.E. Williams, *Sens. Actuators B* **1** (1990) 113

[6] Our set-up allows also to determine photo-induced effects.

[7] J.Szöko, A.Berkó, *Vacuum* **71** (2003) 193–199

current at a constant value (0.6 nA) which corresponds to an initial tip-cluster spacing, z_0. A large number of current-voltage curves are taken, to provide a better statistics of the *I-V* data. The distance is then decreased by a small value Δz of 0.1 Å and *I-V*-curves are determined. This is repeated until a contact between the tip and the cluster is formed. Thermal drifts, leading to lateral shifts of the tip with respect to the cluster, are checked by taking images of the area of interest at low-resolution and hence short acquisition time. In case of a significant displacement, the tip is re-positioned at approximately the initial location. We noticed that the Pt clusters behave mechanically soft in accordance to the macroscopic behaviour of Pt so that the W tip remains in good order while the tip is also damaged when touching the harder TiO_2 surface. Figure 2 shows a series of ln *I-V*-curves as a function of tip-cluster spacing Δz. On the yellowish plane, the ln *I* /*s*. Δz curve is displayed together with a confidence regime of ±95%. The dashed straight line indicates the linear relationship between ln *I* and Δz for tunneling through a constant barrier of 5 eV. Only in the beginning of the approach (approx. until 200 pm) the experimental data would be in accordance with a such a simple model. For larger values of Δz, however, the slope of the linear fit suggests that the interaction between the W tip and the Pt nanocrystal is of chemical nature, as expected when a contact is formed.

The second improvement of the experimental set-up concerns an oxygen source which is needed to expose the "nanodiode" to O_2. This gas has been found to strongly influence the *I-V*-curves of macroscopic Pt/TiO_2 diodes, indicating the sensor effect of related devices.

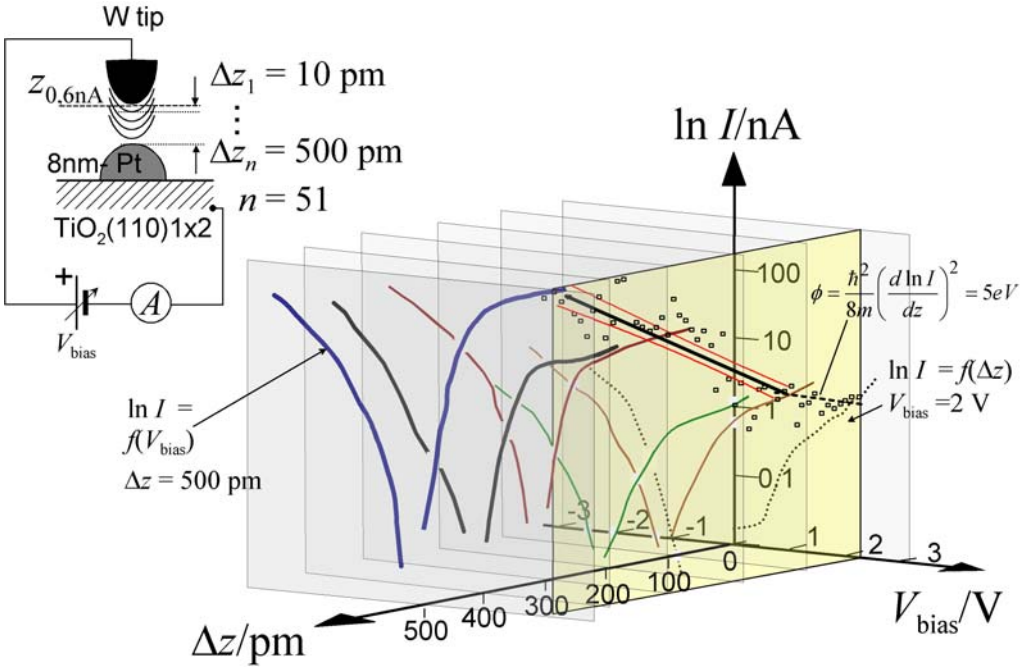

Figure 2. *I-V*-curves of a single Pt cluster on TiO_2 (110).

We have explored mainly two arrangements with oxygen sources in order to introduce oxygen into the uhv chamber without using a leak valve; such a valve cannot be used because of the mechanical disturbance and the likelihood of resulting in significant tip-cluster displacements. The best results have been obtained with an ion pump-type of valve that utilizes the high oxygen diffusion of a heated yttria-stabilized zirconia single-ended tube (Figure 3 *top*). The oxygen flow can be controlled by the temperature and the voltage that is applied over the internal and the external Pt contacts of the tube.

A typical result of the oxygen pressure in the uhv chamber, adjusted by different voltages and different heating currents, as a function of time is shown in the bottom image of Figure 3. The data confirm that a sufficient high pressure can be achieved just by switching; a mechanical disturbance cannot occur because of the operation principle.

The *I-V*-curves shown in the Figure 4 present the first experimental evidence that the nanosized diode structures change their electrical behaviour as the result of oxygen exposure.

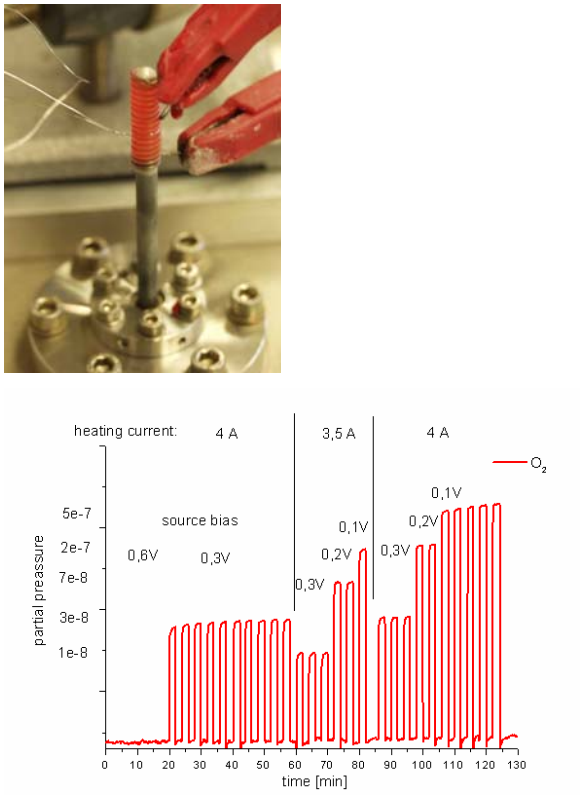

Figure 3. *Top:* Photo of the oxygen-pump attached to the uhv-STM. It shows the flange connector and the outer heating wire to adjust the ion conductance of the YSZ-tube. *Bottom:* Oxygen pump in action.

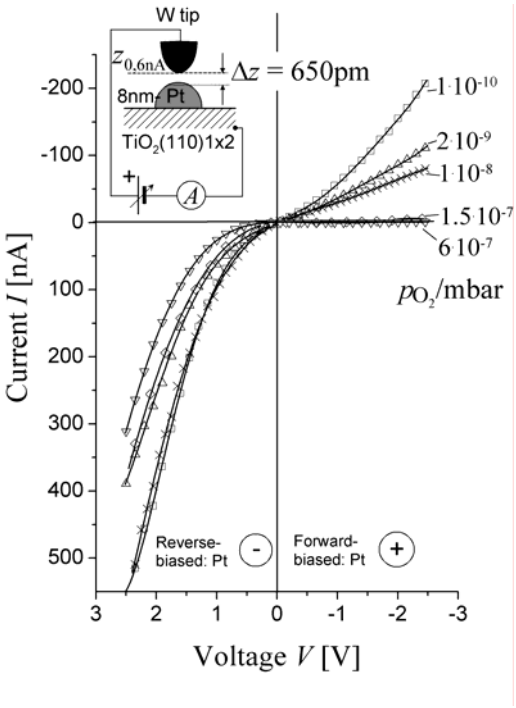

Figure 4. *I-V* curves of nanosized Pt clusters on TiO_2 measured with an STM in tip/cluster contact. The tip is approached by 650 pm from the pre-adjusted position $z_{0.6nA}$ towards the Pt particle.

It shows that the structures behave like non-linear circuit units in uhv (as expected for reduced TiO_2) but converts into Schottky-diodes upon O_2 interaction. The net effect corresponds to the behaviour of macroscopically Pt contacts on TiO_2(110) single crystals.[8] Further experiments must explore the effect of the nanometer dimensions on the *I-V*-shift (which should be related to the length of the three-phase boundary) and on the dynamics of the O_2 response (which should be related to the kinetics of the involved surface reactions and space-charge built-up).

To summarize, we have been able to prepare "prototypical" nano-sized Pt/TiO_2 structures, image them with scanning tunneling microsocpy and build an experimental set-up for contacting individual Pt clusters, localized on-top of the TiO_2 surface. *I-V*-curves can be determined of such nanostructures. An oxygen pump, necessary to expose oxygen to the nanostructures, was developed and implemented to the STM chamber. First results of the oxygen sensing properties of such nanoscopic diode structures have been received.

Apart from addressing single clusters, scanning tunneling microscopy provide also insights to *molecular interactions with TiO_2(110) surfaces* that are relevant in the context of cross-sensitivity of oxide sensors towards humidity. We identified that the reactivity of TiO_2 against oxygen at room-temperature was caused by the surface hydroxyls, which are present even under UHV conditions if the surface is not freshly prepared. Some basic processes are indicated in Figure 5.

[8] U. Kirner, K.D. Schierbaum, W. Göpel, L. Leibold, N. Nicoloso, W. Weppner, D. Fischer and W. Chu, *Sensors and Actuators B* **1** (1990) 103 - 107

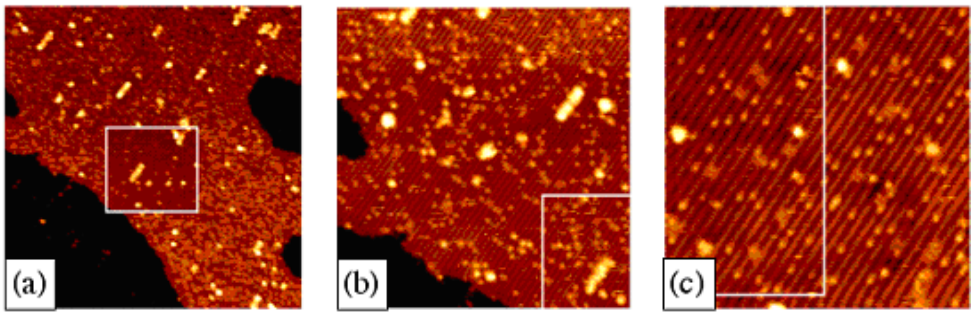

Figure 5. STM images of the reaction of molecular oxygen with the TiO_2(110) surface.

(a) Starting with a hydroxylated surface, the vast majority of was removed from highlighted area by scanning with a voltage of 3V. (b-c) After exposure to 90 L O_2; the previously patterned area is highlighted. We confirmed that after exposure of a TiO_2(110) surface containing bridging hydroxyls to 2 L of molecular oxygen the vast majority of the hydroxyls at bridging sites bridging OH_{br} is removed and some new sporadic adsorbates appear on five-fold coordinated Ti_{5c} sites. These new adsorbates could be assigned to atomic O, OH on Ti_{5c}, H_2O_2 and/or O_2H, which is related to the water chemistry and is important for gas sensing properties.

Another topic of relevance for oxides is the *doping by surface additives* (compare Figure 1b). We have chosen molybdenium as a metal that can adopt different oxidations states and consequently provide insight in a broad range in possible sensor/additive surface interactions. The behaviour of Mo thin films on TiO_2(110) was studied by photoemission XPD and STM experiments. Two different Mo sources were used for the preparation of the thin films: a standard e-beam evaporation source and and organic compound, $Mo(CO)_6$. In the first case it was found that when a highly defective, blu TiO_2 sample is used (blue-TiO_2) as substrate, a thermal treatment in UHV allows the formation of MoO_x structures only at very low coverages (lower than 0.5 eqML), while at higher coverages the very strong Mo-Mo interactions always leads to the formation of a Mo(100) epitaxial film.[9] The formation of MoO_x structures, at low coverages, was confirmed by XPD measurements where it was shown that the Mo atoms are substituting the last layer Ti ions bound to the bridging oxygens. This tendency of Mo to substitute some of the Ti^{4+} ions of the outermost layer was also confirmed by DFT calculations. Thus, an interface layer reminescent of the MoO_2 structure (which has a distorted rutile structure) is formed. The STM measurement showed that, when 1 or 3 Mo eq MLs are deposited, an annealing treatment to 950 – 1000 K leads to the formation of Mo clusters having sizes in a very wide range (1 – 20 nm).[10] The *dI/dV* STS spectra did not display the local electron density of states of Mo clusters, thus indicating the formation of a Schottky barrier in the cluster substrate interface region.

If instead, a $Mo(CO)_6$ source was used there was a clear evidence for the formation of a MoO_2 overlayer having a defined epitaxial relation with the substrate. In this case the $Mo(CO)_6$ decomposition was obtained in a reactive atmosphere (8 x 10^{-6} mbar O_2) and with a hot TiO_2(110) substrate. This procedure was effective only in the case of a defective blue-TiO_2 substrate, while in the case of a new yellow-TiO_2 surface it was rather difficult to decompose the $Mo(CO)_6$ precursor in the same conditions (TiO_2 surface at 700 K in a 8 x 10^{-6} O_2 atmosphere) and a mixture of products was obtained (MoO_2 and MoO_3) . Finally if a deposition of a thick Mo on blue-TiO_2 film in UHV followed by a 30' thermal treatments in air lead to the formation of a near surface alloy where the Mo^{4+} ions are embedded into the TiO_2 lattice as proven by XPD measurements.[11] The amount of Mo in the alloy was found to be less than 10%. Thus, this procedure allowed to obtain a TiO_2(110) surface doped with an electron rich element.

---

[9] B. Domenichini, G.A. Rizzi, P. Krüger, M. Della Negra, Z. Li, M. Petukhov, G. Granozzi, P.J. Møller, S. Bourgeois, *Phys. Rev. B* **73** (2006) 245433

[10] M. Petukhov, G.A. Rizzi, B. Domenichini, G. Granozzi, S. Bourgeois, accepted for publication in *Surf. Sci.*, Dec. 2006

[11] G. A. Rizzi, A. E. Reeder , S. Agnoli, G. Granozzi, *Surf. Sci.* **600** (2006) 3345

In principle such an experimental approach should also be possible to look at the local *I-V*-curves of $Cr_{1.8}Ti_{0.2}O_3/TiO_2$, as initially planned. However, because of the delay in the development of the corresponding experimental set-up, measurements on this system were restricted to Cr/TiO_2.

3 pn Junctions

Figure 3 indicates an idealized sensor structure of a p-type (CuO) and n-type (ZnO) oxide. The potential of such systems is related to the fact tha CuO-modified SnO_2 sensors show a surprisingly high sensitivity and selectivity of towards H_2S; the effect is related to p-type (CuO) – n-type (SnO_2) interface.[12,13]

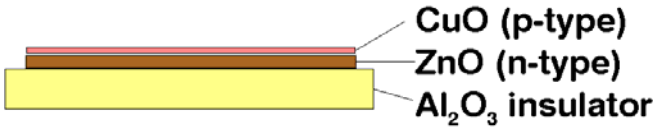

Figure 6. Idealized sensor structure with an interface between a p- and n-type oxide. Applicable sensors must be composed of interfaces that are accessible to detected gas molecules.

However, model systems for surface science studies were not known at the beginning of the project. We have chosen a recipe for ZnO epitaxial thin films that is based on an epitaxal film of Al_2O_3(0001) on a Ni_3Al(111) single-crystal surface. The two main innovations were made to achieve epitaxial growth of ZnO. First, pressed powder ZnO specimen was used instead of metallic zinc as a source for evaporation. This way we have avoided UHV facility contamination. Moreover, deposition technique using already oxidized precursor required lower reactivity of residual oxygen during film growth process, which means that we could use gas oxygen instead of plasma source. Second, the new template for epitaxial growth: oxidized Ni_3Al(111) surface. From our previous STM studies we have found that thin layer (5Å thick) of Al_2O_3 with a perfectly flat and ordered (0001) surface which forms after oxidization of Ni_3Al(111) surface is ideal for thin film growth with roughness possibly in ångstrom range. Low film roughness is essential in order to achieve sharp interface between p-type and n-type layers. The performance of the p-n junction is based on the sharpness of the interface.

We have continue the development and improvement of the recipe for ZnO epitaxial thin films grown on Al_2O_3(0001)/Ni_3Al(111) surface. Additional synchrotron beam time at the ISA facility at University of Århus was essential in order to perform Photoemission (PE) spectroscopy measurement as a support for Scanning Tunneling Microscopy (STM) and Low Energy Electron Diffraction (LEED) studies made at University of Copenhagen. Finally, we have established optimal conditions for ZnO epitaxial thin film growth using reactive deposition technique.

The two main innovations were made to achieve epitaxial growth. First, pressed powder ZnO specimen was used instead of metallic zinc as a source for evaporation. This way we have avoided UHV facility contamination. Moreover, deposition technique using already oxidized precursor required lower reactivity of residual oxygen during film growth process, which means that we could use gas oxygen instead of plasma source. Second, the new template for epitaxial growth: oxidized Ni_3Al(111) surface. From our previous STM studies we have found that thin layer (5Å thick) of Al_2O_3 with a perfectly flat and ordered (0001) surface which forms after oxidization of Ni_3Al(111) surface is ideal for thin film growth with roughness possibly in ångstrom range. Low film roughness is essential in order to achieve sharp interface between p-type and n-type layers. The performance of the p-n junction is based on the sharpness of the interface.

[12] A. Galdikas, A. Mironas, D. Senuliene, A. Setkus, W. Göpel, K.D. Schierbaum, *Sens. Actuators B (Chem)* **58** (1999) 330

[13] J. Liu et al., *Sensors* **3** (2003) 110

We have investigated the early stages of ZnO thin film growth. The stepwise deposition was made at room temperature (RT) and the annealing in oxygen was performed after each step. As the thickness of the film grows the temperature can be raised up to 725K. The annealing temperature above 800K leads to film decomposition into metallic phase. The Figure 7 presence the STM images for growth of 5nm thick ZnO layer. For the RT deposited layers we have no observation of long range order by the LEED, but after the first annealing in oxygen the 5 nm thick layer start to show the hexagonal pattern (see insets in STM images at Figure 7).

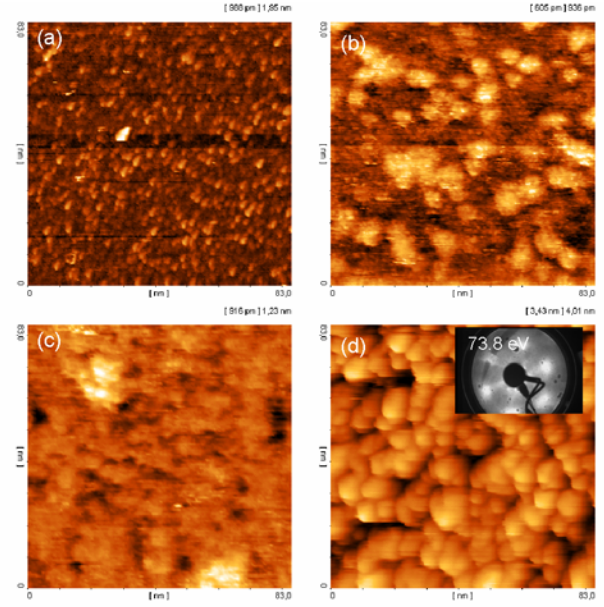

Figure 7. STM images of early stages of ZnO layer growth. Each image shows 83x83 nm2 area. (a) 0.3 nm thick layer deposited at RT (b) 1 nm deposition at RT (c) 2 mn at RT (d) 5 nm deposited at RT followed by the annealing in $1.2*10^{-5}$ mbar of O_2 at 725K.

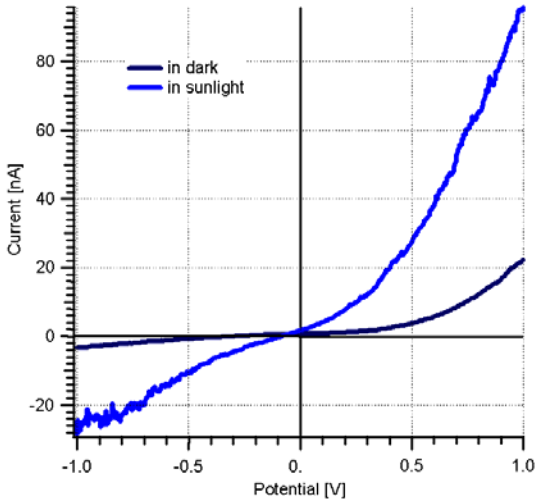

Figure 8. I/V characteristic for p-n junction made of 15 nm ZnO and 5 nm Cu_2O epitaxial layers measured in air.

On top of the ZnO layer the Cu in oxygen was deposited at 425K. The PE spectroscopy shows that even at highest possible O_2 partial pressure for our UHV system ($5 \cdot 10^{-5}$ mbar) we could not achieve CuO stoichiometry but only Cu_2O phase. We could not exceed 450K for reactive Cu deposition because of strong mixing at the films interface. Nevertheless, Cu_2O is a perfect candidate for junction because it is also n-type conductor. Moreover, between Cu_2O(111) and ZnO(0001) surfaces there is a perfect epitaxial match which leads to improvement of long range order and sharp p-n interface.

As the final step, sample composed of 15 nm thick ZnO layer and 5 nm Cu_2O overlayer was removed from the UHV facility in order to measure voltage-to-current (I/V) characteristics. At the Figure 8 I/V curve measured in air using standard one-point method shows Schottky diode characteristics for low voltaic ranges. Moreover, created p-n junction found to be light sensitive.

4 Epitaxial and thin layers

Figure 9 displays a novel type of sensor structure, making use of tunneling through a thin chemically sensitive dielectric oxide. Related sensor devices and systems, based on $Au/Al_2O_3/Au$ have been studied for SO_2 sensing.[14] We explore the use of homo- (WO_3/W) and heteroepitaxial systems (TiO_x/Pt). A further goal the research was to prepare well-defined model

[14] K.M. Donnelly et al., *Meas. Sci.Technol.* **13** (2002) N57

system to investigate the fundamental properties and dependences of metal oxides used in chemical gas sensors.

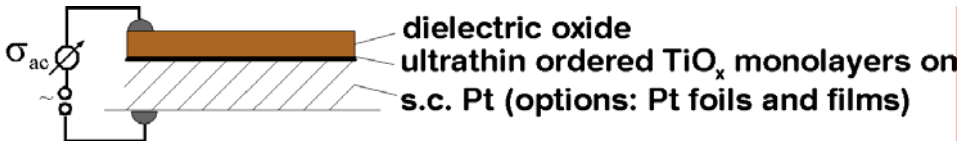

Figure 9. A hypothetical tunneling device, comprising dielectric oxides, ultrathin TiO_x monolayers and a metallic substrate.

The preparation of epitaxial WO_x/W(110) layers followed the 2nd-year work in which we mainly investigated polycrystalline and partially oriented tungsten oxide layers prepared on non-conductive substrates. Such systems, although of interest for semiconducting sensors (see below), show strong charging effects during measurements with electron spectroscopies. The WO_x/W(110) was prepared by oxidation of a (110) tungsten single-crystal under a vacuum using radiofrequency (RF) oxygen plasma treatment.

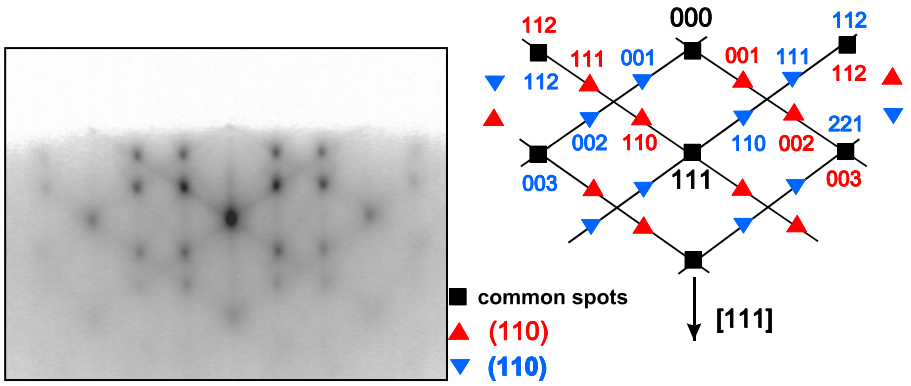

Figure 10. RHEED diffraction pattern and its interpretation from tungsten oxide epitaxial layer prepared on (110) surface of tungsten single-crystal.

The procedure consisted of the oxidation of the W(110) surface at room temperature followed by heating of the sample at 630°C in ultra high vacuum (UHV). The example of surface structural analysis is shown in the

Figure 10.

The RHEED (Reflection High-Energy Electron Diffraction) results confirm the presence of epitaxial WO_3 crystal grains on the surface showing an (111) epitaxial plane. Although the heating of the sample under UHV led to partial reduction, the WO_3 structure was preserved and the lack of oxygen atoms in the layer is compensated by formation of crystallographic shear planes. In addition, the low thickness of oxide layer prevents the charging effect during spectroscopic measurements.

The chemical properties of the sensors are often modified by doping of the sensor surface by any active metal. In our case we used a small amount of Pd. The two phases of metal clusters, (111) epitaxial and non-oriented were found.[15] The electronic structure of the above mentioned systems was investigated by SRPES (Synchrotron Radiation Photoelectron Spectroscopy) at Syncrotrone Elettra in Trieste.[16] During these measurements the structure of the system was checked by LEED. The electronic structure was determined mainly from the form of W4f and

[15] K. Mašek, S. Nemšák, V. Matolín, *Vacuum*, accepted 2007

[16] K. Mašek, J. Libra, T. Skála, M. Cabala, V. Matolín, V. Cháb, K.C. Prince, *Surf. Sci.* **600** (2006) 1624

valence band spectra. The example of evolution of W4f spectra at different steps of experiment is shown in the Figure 11. Deconvolution of the spectra permits to recognize different oxidation states of tungsten and their evolution after the redox treatments. Mainly the W^{6+}, W^{5+}, W^{4+} and W^{0} states were found. The reactivity of clean as well as doped surfaces was checked by interaction with simple molecules like oxygen and carbon monoxide. The unexpected behavior was observed in the case Pd doped surfaces. It is caused by metal substrate interaction.

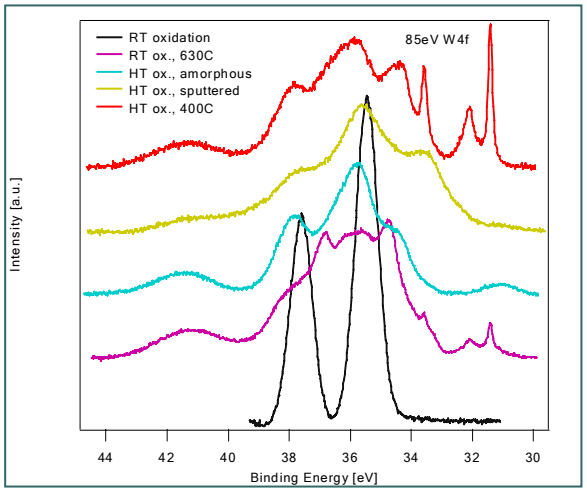

Figure 11. W4f photoemission spectra (SRPES) taken at primary photon beam energy of 85eV at different steps of experiment.

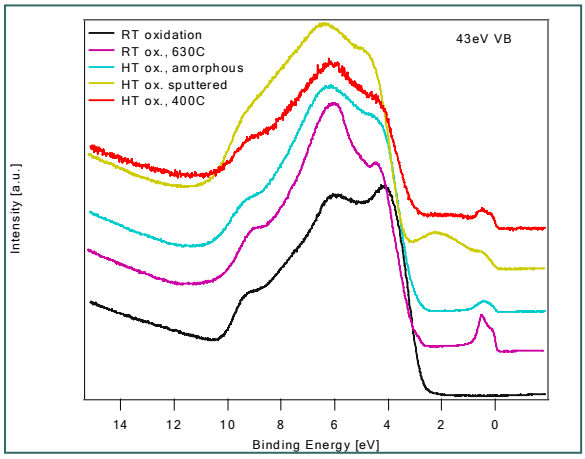

Figure 12. Valence band photoemission spectra (SRPES) taken at primary photon beam energy of 43eV at different steps of experiment.

The reactivity of surface can be deduced from the valence band spectra. Evolution of valence band spectra after different treatments is presented in the Figure 12. The spectrum can be decomposed into three components corresponding to the W5d, O2p and hybridized states. In addition, other states corresponding to the active metal can be observed near the Fermi edge. The role of different species in the valence band region was investigated by resonance photoemission spectroscopy. It gave very interesting results which are not completely understood yet and requires further investigation.

Another model system of the NanoChemSens project is TiO_x/Pt. We explored two different surfaces of a single crystal Pt namely the (111) and the (110) surface. Since the start of the project it appeared soon that the structure of such an ultrathin TiO_2 system is by far more complex that it was known at that time. We found many different phases in the ultrathin film regime obtained by reactive evaporation of Ti in an oxidative ambient. The main difficulty was that, if not optimised deposition conditions were adopted, several nanophases were actually present. During the first year the procedures for the reactive deposition of the TiO_x films have been studied, with particular emphasis on the high coverage regime. In these conditions, titania stoichiometric 3D epitaxial clusters were obtained which were characterized by several surface science tools (photoemission, electron diffraction at low energies, LEED, angle-scanned photoelectron diffraction, XPD, scanning tunneling microscopy, STM). The interesting and surprising outcome was that the 3D clusters were azimuthally ordered (as demonstrated by their XPD patterns) and this means that the during the first stages of deposition some templating layers were obtained.[17] After a patient optimization procedure we eventually found the correct recipes for obtaining almost pure nanophases.

[17] F. Sedona, M. Eusebio, G. A. Rizzi, G. Granozzi, D. Ostermann and K. Schierbaum, *Phys. Chem. Chem. Phys*. 7 (2005) 697.

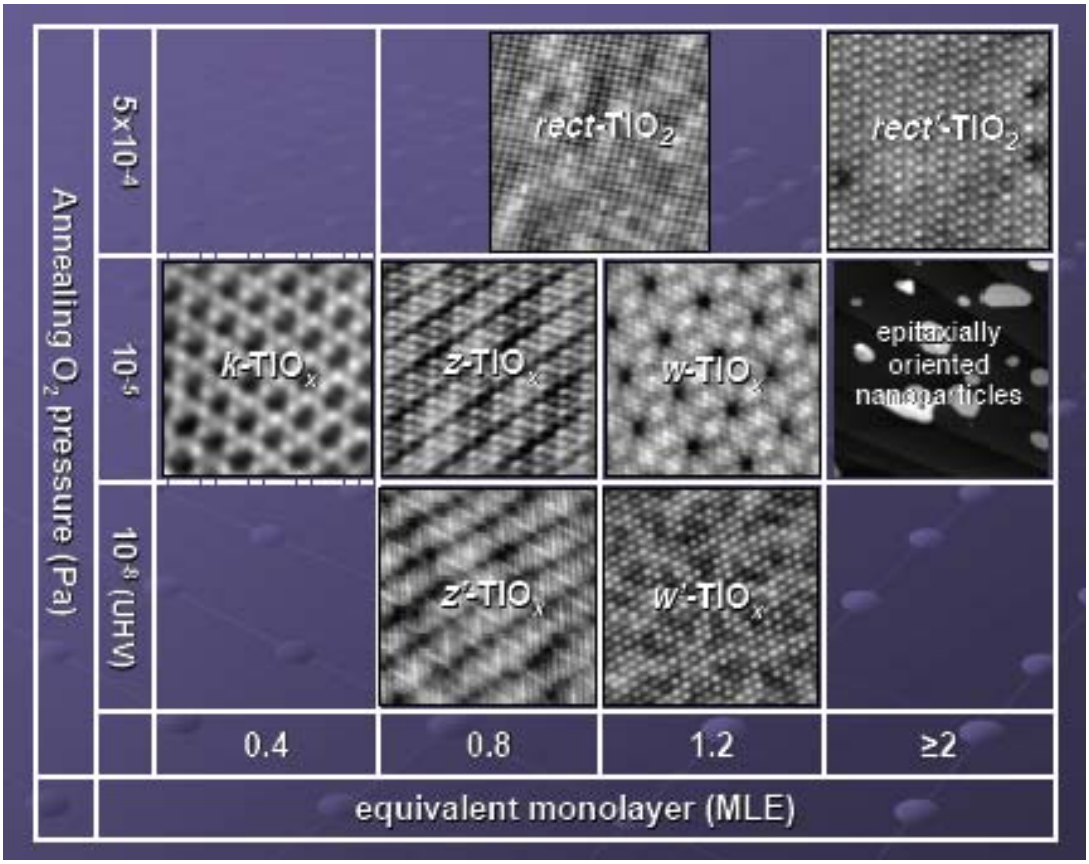

Table 1. The different TiO_x/Pt(111) nanophases obtained after different post-annealing treatments.

In Table 1 we report the STM images of the whole set of nanophases which have been prepared and characterized. By varying the Ti dose and the annealing conditions (i.e. temperature and oxygen pressure), seven different long-range ordered phases were obtained. They were characterized by LEED), XPS STM. By careful optimization of the preparative parameters we have found conditions where predominantly single-phases of TiO_x, revealing distinct LEED pattern and STM images, are produced. XPS binding energy and XPD data indicated that all the phases, except two (the stoichiometric *rect*-TiO_2 and *rect'*-TiO_2), were one-monolayer thick and composed of a Ti-O bilayer with interfacial Ti. Atomically resolved STM images confirm that confirm that these TiO_x phases wet the Pt surface, in contrast to the stoichiometric ones. This indicates their interface stabilization. At a low Ti dose (0.4 monolayer equivalents, MLE), an incommensurate *kagomé*-like low density phase (*k*-TiO_x phase) was observed where hexagons are sharing their vertices. At a higher Ti dose (0.8 MLE) two denser phases were found, both characterized by a zigzag motif (*z*- and *z'*-TiO_x phases), but with distinct rectangular, commensurate unit cells. Among them *z'*-TiO_x, which is obtained by annealing in UHV, shows a larger unit cell. When the post-annealing of the 0.8 MLE deposit is carried out at high temperatures and high oxygen partial pressures, the incommensurate non-wetting fully oxidized *rect*-TiO_2 is found At a higher coverage (1.2 MLE), two commensurate hexagonal phases are formed, namely the *w*- [$(\sqrt{43}\times\sqrt{43})$ *R* 7.6°] and *w'*-TiO_x phase [(7×7) *R* 21.8°]. They show *wagon-wheel-like* structures and have slightly different lattice dimensions.[18] Subsequently, a further wagon-wheel-like monolayer phase have been prepared and the whole set of three phases completely characterized by STM and LEED (see Figure 13). Their STM contrast has been interpreted on the basis of a Moiré-like pattern.[19]

[18] F. Sedona, G.A.Rizzi, S. Agnoli, F. X. Llabrés i Xamena, A. Papageorgiou, D. Ostermann, M. Sambi, P. Finetti, K. Schierbaum and G Granozzi, *J. Phys. Chem. B* **109** (2005) 24411.

[19] F. Sedona, S. Agnoli, G. Granozzi, *J. Phys. Chem. B* **110** (2006) 15359.

Looking at the last two columns of the Table reported above, it is easy to see how the hexagonal mesh of the overlayer changes after a reducing annealing. Actually, starting from the *w*-TiO*x* phase (unit cell 3.26 Å and θ 1.36°), after an ultrahigh vacuum (UHV) annealing the hexagonal mesh shrinks and rotates with respect to the Pt(111) substrate, obtaining the w_{int}-TiO*x* phase (unit cell 3.23 Å and θ 3.3°), and finally the *w*'-TiO*x* phase (unit cell 3.18 Å and θ 3.5°). An interpretation of this phenomenon has been put forward.

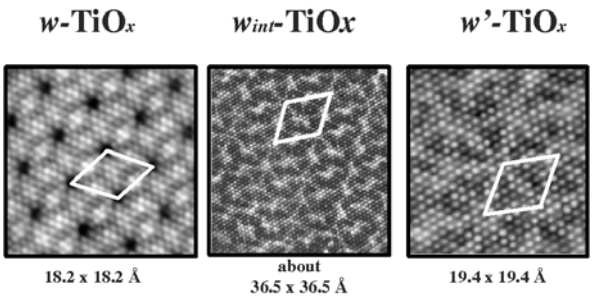

Phase	*Wood notation*	*Supercell dimension*	*Overlayer Unit cell dimension*	*rotation film /substrate*
w-TiOx (most oxidized)	(√43 × √43) *R* 7.6°	18.2 Å	3.26 Å	1.36°
w_{int}-TiOx	(√175 × √175) *R* 19.1°	36.5 Å	3.23 Å	3.3°
w'-TiOx (most reduced)	(7 × 7) *R* 21.79°	19.4 Å	3.18 Å	3.5°

Figure 13. The three wagon-wheel phases of ultrathin TiO_x.

The data of three synchrotron radiation runs at ELETTRA (Material Science beamline, Trieste) carried out in collaboration with the UDUS and PRA research units have been interpreted and a consistent picture of the electronic structure of the whole set of nanophases has been put forward.[20] In particular, the valence band (VB-PES) data appear to be sensitive to the details of the film structure by also displaying electronic features that are particular to each individual film (see Figure 14). It turns out that mixing with Pt states plays a major role in determining the electronic structure of the reduced substoichiometric films, whose spectral data are also consistent with a stoichiometry close to TiO and with the presence of a Ti-Pt interface. This finding is in agreement with previously reported photoelectron diffraction data. The stoichiometric films show a valence band structure that is strongly reminiscent of the one measured on the stoichiometric bulk TiO_2 surface. Deviations from the bulk band structure appear in the form of a narrowing of the band and in a shift toward lower binding energy. The band narrowing effect is attributed to the spatial confinement of the TiO_2-like films, while the shift is attributed to mixing of film and Pt substrate derived states.

[20] P. Finetti, F. Sedona, G. A. Rizzi, U. Mick, F. Sutara, M. Svec, V.Matolin, K. Schierbaum and G. Granozzi, *J. Phys. Chem. C* 111 (2007) 869.

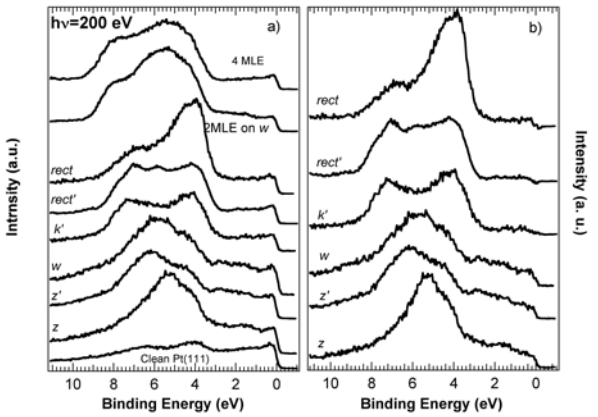

Figure 14. (a) VB-PES data of TiOx ultrathin films on Pt(111) acquired with a photon energy of 200 eV. All data are normalized to the photon flux; (b) Some of the VB spectra after subtraction of a normalized clean Pt(111) spectrum.

The structure of a *zigzag-like* phase (namely the *z*-TiO_x) has been completely resolved and a model (see Figure 15) which fits nicely the STM data has been proposed.[21] The structural model, which is in tune with the whole set of experimental data, has been obtained by a DFT geometry optimization starting from a guessed structure proposed on the basis of chemical considerations and the comparison with literature data. The stoichiometry of the monolayer is Ti_6O_8 and the Ti atoms are formally in the +2.7 oxidation state, in agreement with the photoemission data. However, two different types of Ti atoms have been found, i.e., Ti atoms coordinated by four oxygen atoms, which give rise to the brighter bumps in the *zigzag-like* STM motif, and Ti atoms coordinated by only three oxygen atoms, which appear darker in the STM images. Analogously, two different types of oxygen atoms can be distinguished, with those lying in the *throughs* of the STM images ("bridge" oxygens) being less coordinated and in a lower oxidation state. The energetics of the interaction of the oxide monolayer with the Pt substrate has been computationally evaluated. Even if the oxide/metal interaction is important in determining the high stability and the structure of the oxide film, it turns that this interaction is only weakly directional, thus justifying the incommensurate nature of the film.

Concerning the nanophases obtained under strongly oxidative conditions, we have found that both *rect*-TiO_2 and *rect'*-TiO_2 present quite unusual structures which are not related to the known bulk-like phases (rutile or anatase). In particular, a similar phase *rect*-TiO_2 with identical dimensions has been prepared on the highly anisotropic Pt(110) substrate as a single-domain phase.[22] By an accurate LEED and STM (see Figure 16) analysis it has been demonstrated that its structural features are identical to those of a lepidocrocite-like nanosheet that can be prepared by the exfoliation of layered titanates using a top-down wet chemistry method. In our case, the nanosheets are assembled in a bottom-up way from the constituent elements and their basic lepidocrocite structure is modulated at the nanoscale due to coincidence with the substrate.

DFT calculations have shown that an isolated lepidocrocite nanosheet is the most stable 2D titania phase, irrespective of the presence of a substrate. Actually, an anatase (001) bilayer spontaneously transforms into a lepidocrocite nanosheet by simply sliding the upper atomic layer with respect to the lower one by half a unit cell along the [100] direction. This involves a shortening of the related unit cell parameter from 0.38 to 0.30 nm, and a substantial energy gain: the lepidocrocite nanosheet is stabilized by 1.24 eV with respect to the anatase bilayer, and turns out to be only marginally less stable (by 0.16 eV/TiO_2) than bulk anatase. This means

[21] G. Barcaro, F. Sedona, A. Fortunelli and G. Granozzi, *J. Phys. Chem*. C 2007 in press.

[22] T. Orzali, M. Casarin, G. Granozzi, M. Sambi and A Vittadini, Phys. Rev. Lett. *97* (2006) 156101.

that it is the reduced dimensionality of the overlayer, rather than the interaction with the substrate, which stabilizes the lepidocrocite structure.

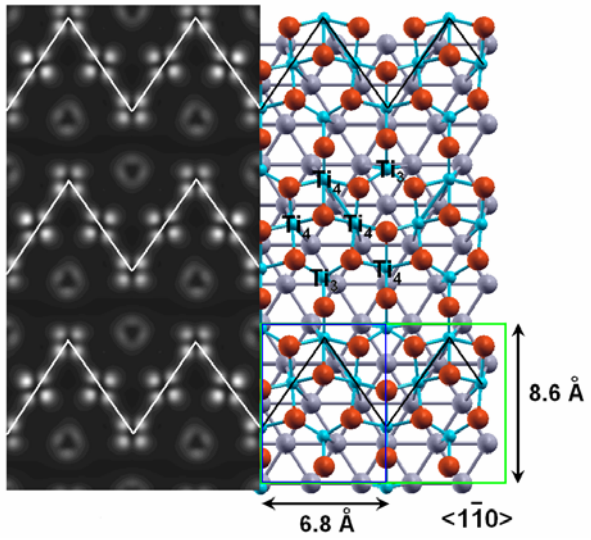

Figure 15. Relaxed structure of the z-TiO_x phase model (right-hand side) and the corresponding simulated STM image at +1.00 V (left-hand side): the STM image is obtained by using 4 Pt layers to describe the metal support; the brighter four-coordinated Ti atoms (denoted as Ti_4 in the figure) draw a zigzag-like motif (underlined) along the $\langle 1\bar{1}0 \rangle$ direction of the support, whereas the three-coordinated Ti atoms (denoted as Ti_3 in the figure) are hardly visible.

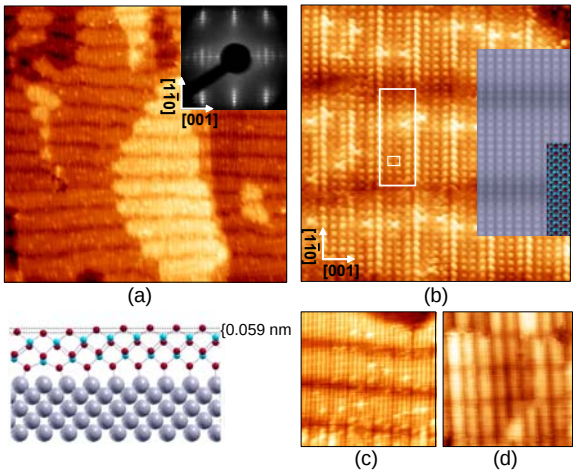

Figure 16. (a) Large area STM image (62 nm x 62 nm; VS=0.48 V; I_T=1.4 nA) of a single domain lepidocrocite nanosheet on (1x2)-Pt (110). The central brighter area is separated from the lower terrace by a substrate monoatomic step. Inset: (14x4) LEED pattern. (b) High resolution STM image (13.7 nm x 13.7 nm; VS=0.28 V; I_T=1.65 nA) of the nanosheet. The overlayer (superstructure) unit cell is indicated by the small (large) rectangle. Inset: Tersoff-Hamann simulation of the STM image with superimposed solid sphere model (Oxygen: red, Titanium:blue). Dark stripes along [001] are due to overlayer bending toward the substrate (see the interface side view in the [001] plane, lower left corner; Pt: large, grey). (c) and (d) High resolution STM images of the nanosheet. (13.6 nm x 13.6 nm; VS= 0.42 V; I_T=0.9 nA and 18.0 nm x 18.0 nm; VS= 1.80 V; I_T=1.0 nA).

A DFT calculation has been also carried out on the incommensurate *rect*-TiO_2 phase on Pt(111).[23] A very nice fit with the valence band data has been obtained and some interesting hints on the peculiar chemical properties of such unusual titania nanophase have been obtained. As an important conclusion, these nanosheet-shaped materials can be regarded as a new class of nanoscale semiconductor with a two-dimensional structure and are expected to achieve advanced functions, such as uni-directional electron or energy transfer. They may also attain higher efficiency of light-energy conversion by diminishing electron-hole recombination.

The rich panorama of the TiO_x nanophases offers the opportunity to study different structures with a well characterized long-range ordered defectivity, so allowing to assess the role of defects in the chemical reactivity of substoichiometric titania-based systems. During the third year we have also made an exploratory study to test their capability as templates for growing ordered and monodispersed metal nanocluster arrays by exploiting the preferential nucleation phenomenon at defects. The ordered array of parallel black troughs spaced by 1.44 nm, observed in the STM data of the *zigzag-like* z'-TiO_x ultrathin film, revealed to be a good template for growing a linear array of Au nanoclusters (see Figure 17).[24]

[23] F. Sedona, P. Finetti, A. Vittadini and G. Granozzi, Yongfan Zhan, L. Giordano and G. Pacchioni, manuscript in preparation.

[24] F. Sedona, S. Agnoli, M. Fanetti, I. Kholmanov, E. Cavaliere, L. Gavioli and G. Granozzi, *J. Phys. Chem. C* in press

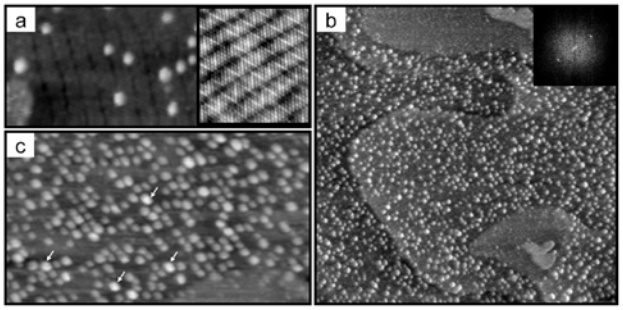

Figure 17. Ordered growth of Au clusters on z'-TiOx phase after annealing @ 550 K: a) lower coverage (0.08 ML) (340 × 140 Å2, V = 0.4 V, I = 0.4 nA), in the inset the original z'-TiOx phase; b) higher coverage (0.35 ML) (1000 × 1000 Å2, V = 0.6 V, I = 0.6 nA). In the inset the Fourier transformation of the image is also reported; c) zoom-in of b) (500 × 280 $Å^2$; V = 0.6 V, I = 1.6 nA).

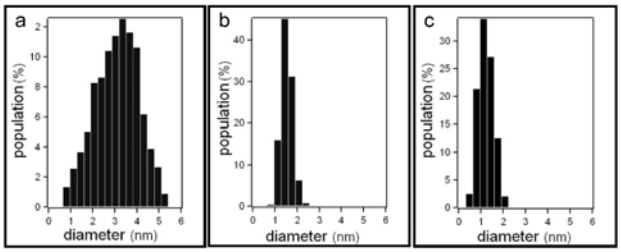

Figure 18. Histograms of the Au clusters distribution for different systems obtained assuming a spherical shape: **a)** *w'*-TiO_x phase, **b)** *z'*-TiO_x after an annealing at 550 K, **c)** *z'*-TiO_x after an annealing at 600 K.

The very interesting point is that the size distribution of the ordered Au nanoclusters is rather narrow (a mean size of 1.3 nm), as evident from the histograms shown in the figure reported below. The *wagon-wheel-like w'*-TiO_x film, having similar chemical composition but without a nanostructured array of defects, does not show templating effects, leading to nucleation of disordered and larger Au clusters (mean size of 3.4 nm with a large dispersion). Hence this evidence shows that the ordering of the deposited Au nanoclusters is strongly dependent on the actual defectivity of the film, directly influencing the Au cluster mobility. The idea of using the intrinsic ordered defectivity of the TiO_x nanophases has allowed us to strongly bind the Au clusters to specific sites determining an effective shape and dimension selection which is retained even at high temperature (600 K). This factor is of fundamental importance in order to overcome the typical restrictions to the use of Au clusters at the catalyst working temperature, which in general induces the sintering of the particles and therefore the loss of their peculiar nano-induced activity.

Moreover, an interesting phenomenon has been demonstrated: we can manipulate an entire array of nanoclusters inducing a cooperative change of their mutual positions by a thermal annealing. Actually, the almost linear array of Au clusters obtained on the *z'*-TiOx template suddenly change to an hexagonal pattern at high temperature (above 600 K) as a consequence of the changes in the ultrathin film template which transform into the *w*-TiO_x one (which presents an hexagonally disposed array of defects). Noteworthy, the transformation occurs without any dimensionality change of the nanoclusters. The important point is that our model system is extremely well suited for a precise investigation of the catalytic activity of the gold nanoparticles on reduced titania within a range of sizes still unexplored.

As the first step towards sensor structures shown in Figure 9, we investigated wheter the ultrathin TiO_x layers are suitable substrates for the growth of layers of ceria (a typical high-k-oxide). This approach is motivated by the fact that the lattice mismatch between the TiO_x and the ceria [CeO_2(111) 1x1, lattice constant *a* = 3.82 Å] surface is lower when compared with metal substrates. The atomic spacing of the w-phase is 3.26 Å; the latter also shows hexagonal symmetry. Metals like Pt, Rh or others have by far smaller lattice constants (typical value approx. 2,8 Å) and correspondingly ceria grown on metallic hexagonal (111) or (0001) surfaces are not well ordered. We have used a Pt(111) sample covered with the z- and w-phase and deposit ceria by reactive evaporation of Ce in oxygen (Figure 19).

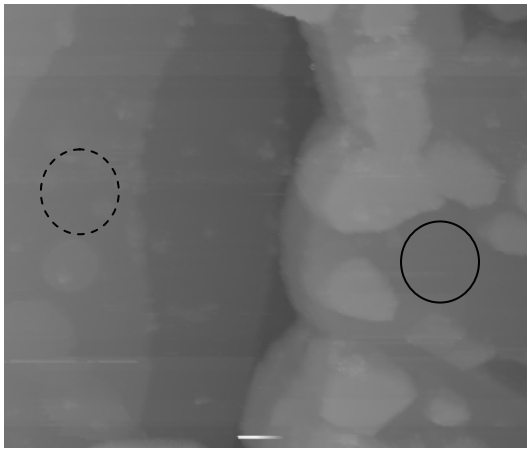

(a)

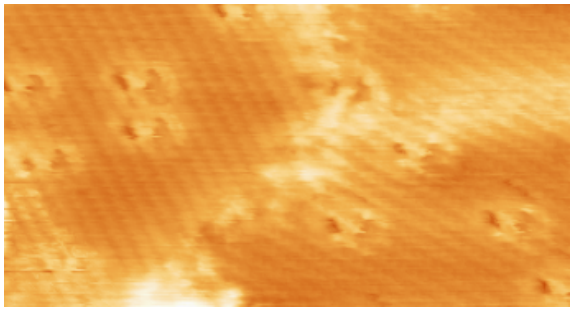

(b)

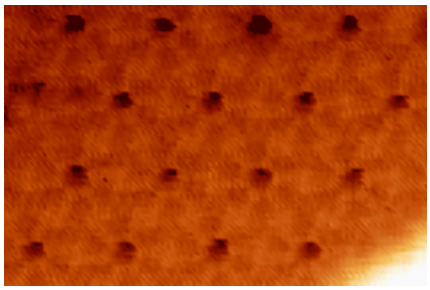

(c)

Figure 19 (a): STM image of the TiOx-phase used for ceria growth (114 x 91 nm², U=2.7 V, I=0.4 nA). Dashed curve: region with w-TiOx (c, 23 x 12 nm², U=2.7 V, I=0.4 nA), solid curve: region with z-phase (b, 10x7.5 nm², U=1.5 V, I=0.4 nA) and TiO_2 clusters.

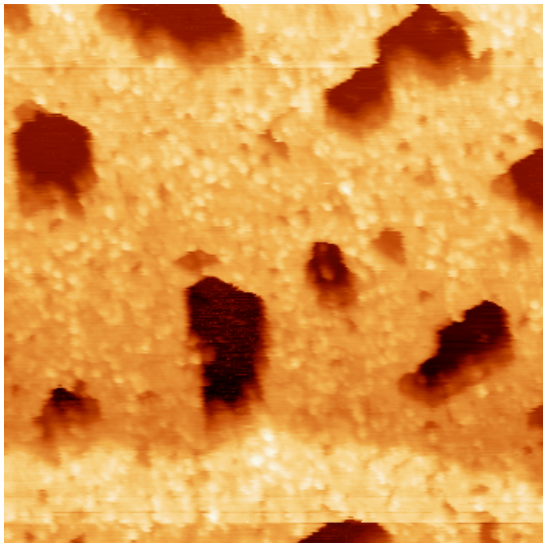

Figure 20. STM image of ceria/TiOx/Pt(111) after a 770 K anneal in oxygen (10^{-7} mbar). 40x40 nm², U=3.2 V, I=0.3 nA.

STM images of the as-received samples show fine and granular ceria, on contrary of goal of this study. However, the substrate coverage completes by an anneal at 770 K (Figure 20). Differences between the different underlying TiO_x phases exist with respect to the film morphology.[25] The ceria/TiO_x/Pt(111) exhibits a flat but not fully closed surface. The surface seems to ordered (at a few spots, hexagonal arranged features can be seen and the 4 Å deep holes show edges with an angular of 120°). However atomically resolved images have not been achieved. Interestingly, annealing at 1100 K in uhv does not lead to a decomposition and allyoing [this reaction occurs with ceria/Pt(111)]; instead a mixed and ordered Ce-Ti oxide is formed.

In an attempt to also explore the growth of TiO_2 on cheaper substrates, we characterised the growth of TiO_2 on Ni(110). During the studies, we found reduced phases of ultrathin rutile TiO_2(110) grown on Ni(110) with STM and LEED. We report the formation of the 1×2

[25] Thorsten Staudt, *diploma thesis,* University of Düsseldorf, 2007.

reconstruction (Figure 21) and crystallographic shear planes consistent with the {132} family of planes (Figure 22 and Figure 23). These phases are assigned by comparison with previous studies of analogous phases on native rutile TiO_2 crystals. As these are bulk defects rather than surface defects we conclude that structurally, the thin films are bulk-like.

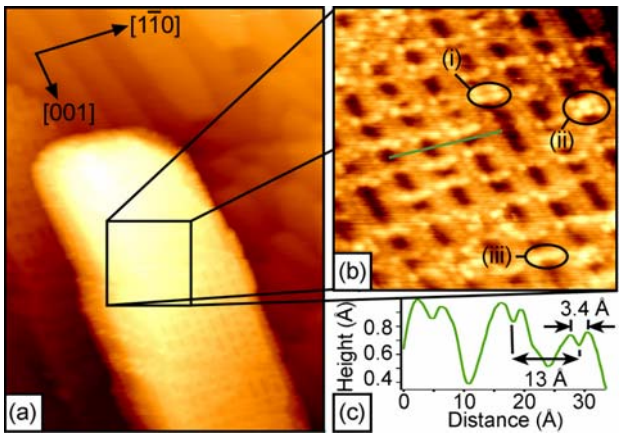

Figure 21. STM images of TiO_2 islands with a 1×2 termination. **(a)** Large scale image (350×470 Å^2, 1.05 V, 3.44 nA). **(b)** High resolution image (93×93 Å^2, 1.00 V, 1.00 nA). Single link (i), cross-link (ii), rosette-link (iii) and the orientation of TiO_2(110) are indicated. **(c)** Line profile along the line drawn in figure (b).

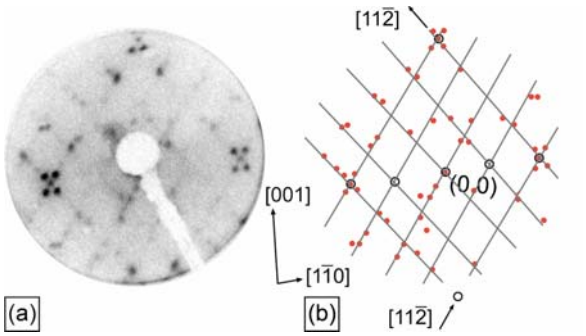

Figure 22 **(a)** LEED pattern (31.9 eV) recorded after annealing the TiO_2 film at 1110 K for 30 min in 1×10^{-7} mbar O_2. **(b)** Schematic diagram of (a) drawn to scale. Filled red circles depict the spots present in the LEED pattern. Open circles show the positions of the 1×1-TiO_2(110) termination. The zero order spot is labelled. The lines indicate the principal directions of the streaking in the LEED pattern referenced against a TiO_2(110) surface unit cell.

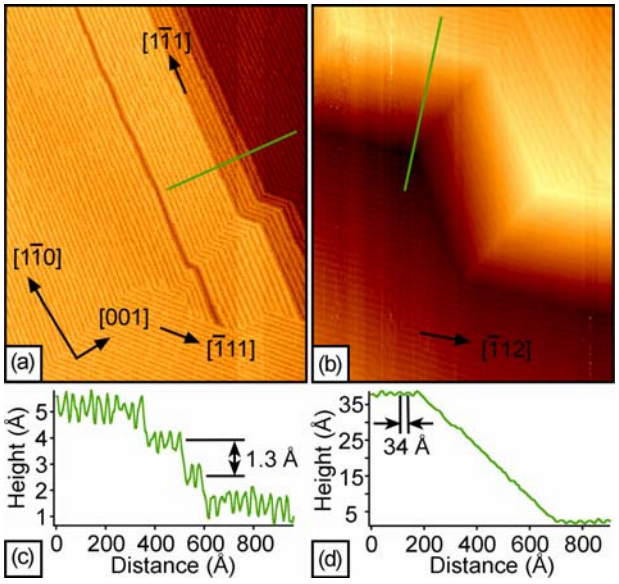

Figure 23. STM images of the topography formed after annealing the TiO_2 film at 1110 K for 30 min in 1×10^{-7} mbar O_2. **(a)** (1692×2115 Å^2, 0.30 V, 0.90 nA). **(b)** (1447×1809 Å^2, 0.15 V, 0.80 nA). The arrows indicate both the principal azimuths of the TiO_2(110) surface and the directions of the CS plane intersections. **(c)** Line profile along the line indicated in (a). **(d)** Line profile along the line indicated in (b).

Figure 24 shows a thin film sensor composed of WO_3 as sensitive layer. This semiconductor is known to be suitable to detect ozone at concentration levels relevant to atmospheric monitoring applications.[26]

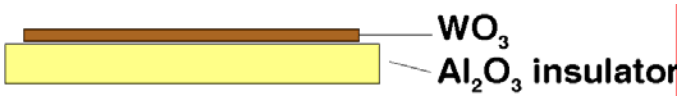

Figure 24. Thin film WO_3 sensor. Another type of sensor is achieved by depositing WO_3 nanorods over suitable devices.

Although WO_3 is already practically applied for sensors, there are no comprehensive reviews like for SnO_2. Exploitation with respect to epitaxial layers or nanostructures are of fundamental importance because of the complexity of the crystal chemistry of WO_3; it shows two different crystalline phases in the range of temperatures where the gas sensors are normally operated (transition temperature from monoclinic to orthorhombic around 330°C).

The WO_3 thin films deposition technique, developed in the second project year, has been used to produce films on sensor prototype structures. They are mounted on special sockets (Figure 25), making them ready for test measurments for NO_2 in our gas flow set-up. We compare the transient of the resistance, obtained during the exposure of small concentrations of NO_2 in N_2/O_2 mixtures of constant humidity,[27] with a commercial electrochemical sensor (Sensoric).

The Figure 26 displays such a measurement. It demonstrates that the films behave as good as the electrochemical device but offers in addition a higher sensitivity at a temperature of 480 K (Figure 27). As the temperature also affects the sensitivity towards humidity changes, it must be well adjusted to give the best compromise between lowest cross-sensitivity for water and highest sensitivity for NO_2.

[26] S R Aliwell *et al* 2001 *Meas. Sci. Technol.* **12** 684-690

[27] humidity effects have also been studied.

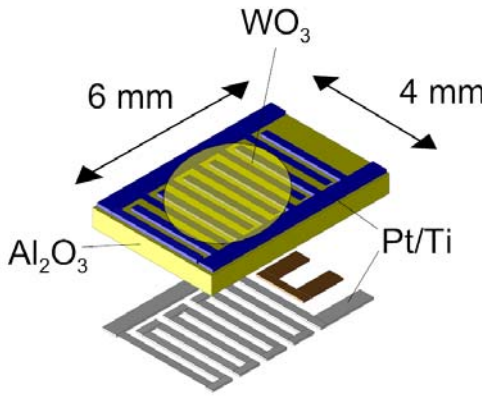

Figure 25. Sketch of the sensor prototype and photograph of the sensor, mounted on a heat-resistant socket (DIL 8 configuration).

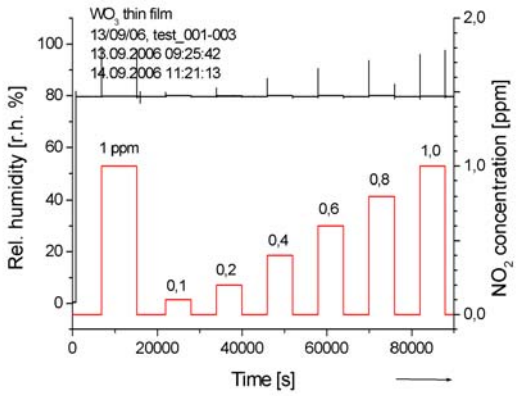

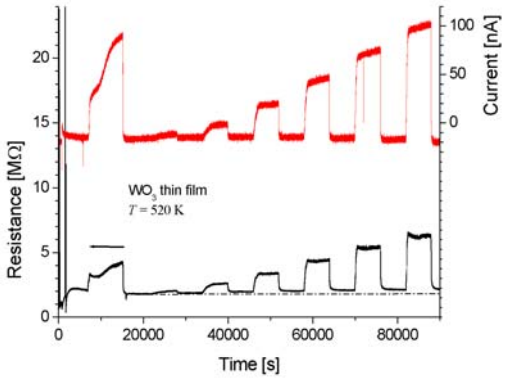

Figure 26. Top: Dosing sequence. Below: Resistance of a thin WO_3 film at T = 520 K and current of a three-electrode electrochemical sensor (red curve) as a function of time.

.

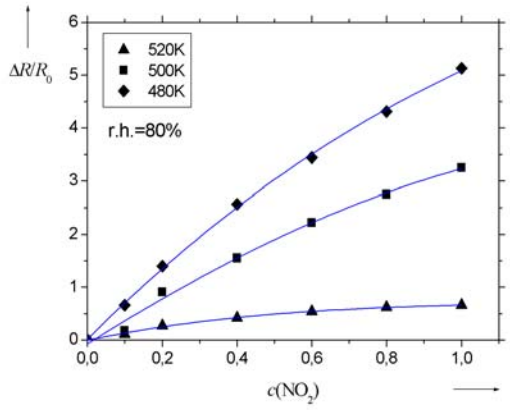

Figure 27. Temperature-dependence of sensor signals (relative resistance change $\Delta R/R_0$) for low concentrations of NO_2. The resistance R_0 is the baseline value without NO_2.

5 Nanorod assemblies

In the context of the NanoChemSens project, WO_3 nanorods are of particular relevance. The high surface-to-bulk ratio of quasi one-dimensional nanostructures is known for well-established sensor materials like SnO_2, ZnO and TiO_2, prepared with self-organized, highly ordered porous anodic alumina (PAO) templates or vapor transport synthesis.[28] A recent report on WO_3 nanorods, deposited over the surface of a MOS device from a colloid solution, confirms the low-temperature NH_3 sensing capabilities of WO_{3-x} nanorods with an interesting conversion of the response characteristics at 370 K (the resistance increases upon NH_3 dosing at temperatures below this value but decreases at higher temperatures). [29]

Recently, some experiments have shown that oxide nanowires present interesting sensing properties in comparison with oxide thin films. Due to their peculiar structure and size effects these materials, commonly denoted as nanowires and nanorods, exhibit novel physical properties. In the field of chemical sensors they are promising candidates because they exhibit a single crystalline structure and a large surface-to-volume ratio, resulting in a complete depletion of carriers inside the nanostructure. These characteristics enhances the role of surface states in the electrical sensor response.

Sensor properties of WO_3 oxide nanowires can be explored, applying two different strategies: The tests can be performed on a single nanowire or on an entire assembly of nanowires. The first route is very promising and has been used with success in some cases demonstrating the specific properties of oxide nanowires. However, this method requires nanomanipulation for the realization of electrical contacts to electrodes, presenting major technical difficulties, or a more complicated preparation process. We will come to this point below. In the next part, we will describe first the second strategy by using self-assembled WO_3 nanowires, electrically connected between two deposited electrodes.

The growth mechanism, established during the second-year work, allowed us to develop a method for obtaining a network of WO_3 nanowires. We have grown them on a mica substrate with a high density. We have demonstrated that such assembled nanowires are well electrically connected to each other and to the two deposited gold electrodes. We studied the sensing response towards CO and NO. We observed a high sensitivity even at relatively low temperature.

Growth of self - assembled WO_3 nanowires

We have evidenced that the growth of WO_3 nanorods on the mica surface is initiated by the formation of a very thin hexagonal tungsten bronze (HTB) compound. This first stage is followed by a layer-by-layer growth of successively hexagonal and monoclinic WO_3 phases. Moreover we observed that the nanorod density is independent of the deposition time.

Starting from these results we deduced that the growth process involves two main phenomena, the formation of an HTB layer and the epitaxy which controls the anisotropic growth. During the oxide deposition, the temperature of the mica substrate is in the range of 360 to 380°C. This corresponds to the temperature of the formation of the HTB according to the reactions:

$$WO_3 + H_2O \rightarrow WO_2(OH)_2$$

$$WO_2(OH)_2 + x\,K \rightarrow K_x WO_3 + H_2O$$

The growth of the HTB phase needs the presence of potassium atoms. The density of the nanowires is independent of the deposition time, this indicates that the HTB nucleation is a fast process which consumes all the K atoms available on the surface. When this happens the growth of the nanowire precursor stops. We have verified this hypothesis in Dijon by thermal desorption experiments. The thermal desorption spectrum from a mica surface shows that in the 340-380°C temperature range most of the potassium atoms desorbs as K or KOH species. So we conclude that we have to supply potassium in compensation of the loss by desorption if we

[28] J. G. Wen et al., *Chem. Phys. Lett.* **372** (2003) 717

[29] Y. S. Kim et al., *Appl. Phys.Lett.* **86** (2005) 213105

want to obtain the nucleation of new population of nanowires. We have proceeded by successive oxide depositions supplying potassium atoms in the vapour source after each deposition run. Electrical conduction measurements have been performed between two electrodes deposited on nanorods prepared by this process. After heating the sample until 250°C the current intensity stabilizes to a value around one nanoampere indicating that the nanowires are self assembled and form an electrical network suitable for sensing tests.

Sensing tests with CO and NO

Figure 28 and Figure 29 show the sensing responses of nanowires towards CO and NO respectively. The tests are realized in a special micro reactor built in Prague under a mixture of oxygen and CO (or NO) at the atmospheric pressure. Prior CO (NO) admittance the sample is annealed in an O_2+argon mixture at 250°C during 12H.

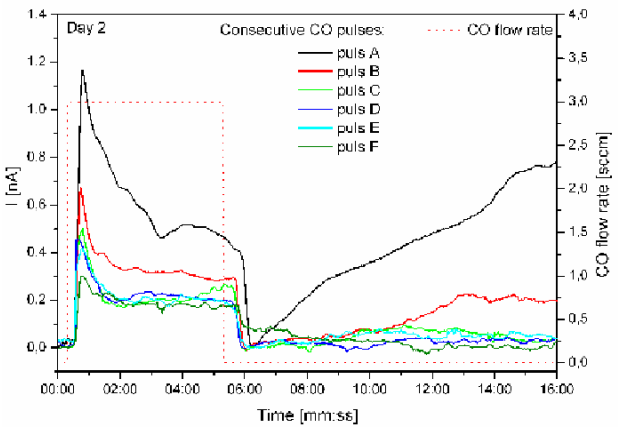

Figure 28. Sensor response of WO_3 needles towards CO.

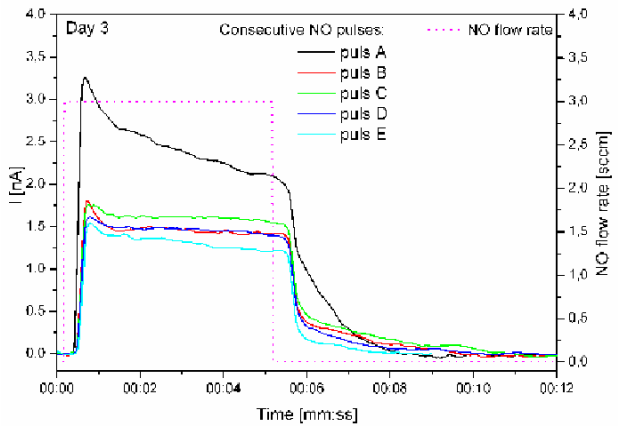

Figure 29. Sensor response of WO_3 needles towards NO.

The responses *I (t)* in the figures were obtained during successive pulses with a flow rate of 3sccm. The main features of the results are

- the responses (excepted after the first pulse) are similar indicating a stable behaviour.
- the response time is short compared to the response given by thin WO_3 films under the same conditions.
- the successive responses exhibit a typical feature (overshoot) which could be tentatively related to the specific structure of the nanowires.

The electronic structure of nanowire assembly and their oxidation states are characterized by XPS in Prague (Elettra) and Dijon. Figure 31 is a typical W4f spectrum obtained with WO_3 nanowires; it exhibits a shoulder on the low energy side which corresponds to the potassium peak of the mica substrate (31 eV). If the contribution of the potassium is removed from the peak one obtained the W4f doublet due to W6+ species with a negligible participation of smaller oxidation states.

It appears that the sensing properties of WO_3 nanowires are not due to the density of oxygen vacancies. In our opinion they should be related to the crystallographic structure of such materials which exhibit specific adsorption sites. According to this hypothesis an interpretation of the results is now in progress.

Further experiments with WO_3 needles have been performed at UDUS. This work focuses also at two-dimensional structures with WO_3 needles, grown on mica. We used 1 μm-electrode arrangement, developed in cooperation with Prof. Th. Heinzel (Institute of Experimental Condensed Matter Physics, University of Düsseldorf). An example is shown in Figure 30. The image shows a network of interconnected WO_3 needles; this type of structure suggests that percolation type of sensors can be developed in principle. Such devices may allow to control the sensitivity through the density of percolation nodes.

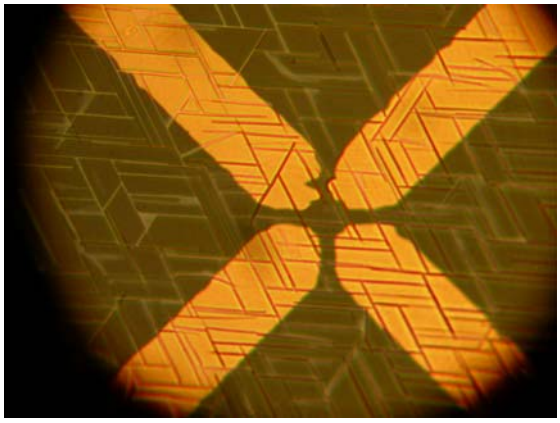

Figure 30. Micrograph of percolation-type sensor based on WO_3. The electrode spacing is approx. 1 µm.

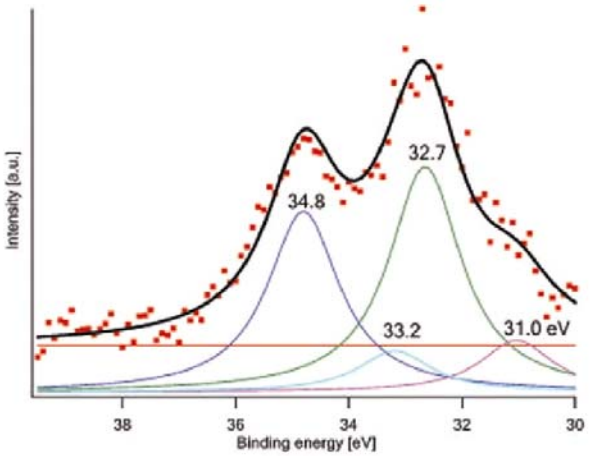

Figure 31. XPS spectrum of WO_3 nanowires.

The mica structures are fixed on the sensor prototype structure (compare Figure 25) and mounted on sockets. By doing so, similar sensing tests could be performed as with the WO_3 thin film sensors. First results of the sensing behaviour of the WO_3 percolation sensor towards NO_2 and H_2O are presented in Figure 32. For the test a short NO_2 pulse (1ppm) is introduced at the beginning to saturate the internal walls of the test equipment. Then, NO_2 concentrations (0.4 ppm) are adjusted at different relative humidities. Finally, NO_2 concentrations are increased from 0.1 ppm until 1 ppm at a fixed relative humidity of 80%. The temperature of the sensor was 200 °C, as determined with a Pt 100 temperature sensor at the backside of the device. The blue graph indicates the sensor response which has be compared with the results of the thin film sensor. Response and decay times are quick and the sensitivity is high. Thee is a slight cross-sensitivity towards H_2O. In conclusion, the data confirm the principal capability of this novel type of WO_3 sensor.

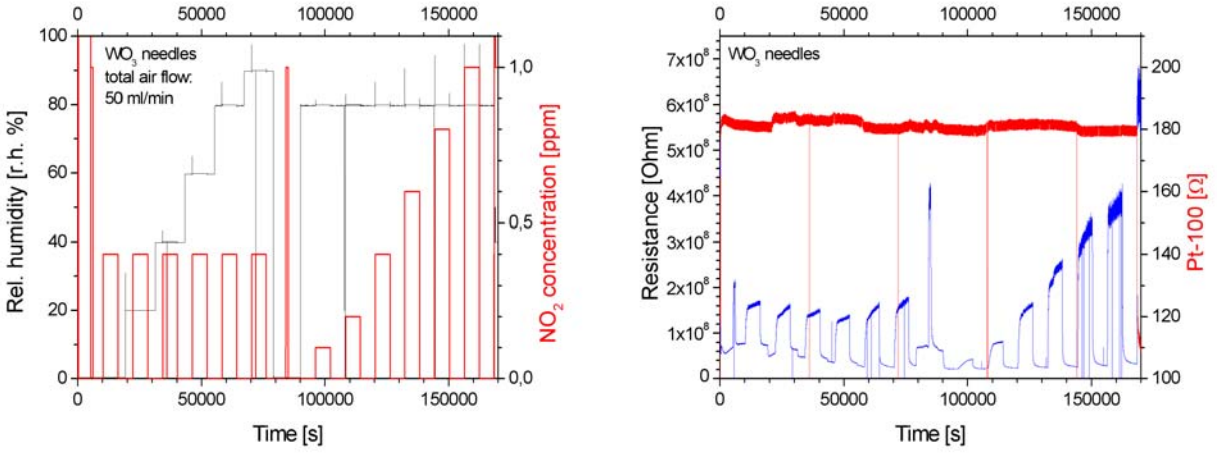

Figure 32. Long-term sensor test of WO_3-based sensor. *Left:* Relative humidity and NO_2 concentrations (red) in air that are exposed to the sensor. *Right:* Pt-100 temperature attached to the backside of the sensor (red) and sensor´s resistance (blue).

6 Functional organic molecules and ionophores for mass-sensitive devices

Figure 33 indicates the use of organic materials with conducting properties that differ from most of the “conventional” inorganic materials. Such molecules have been studied in connection to their sensing properties in the past, indicating partly very high sensitivities to oxidizing gases like nitrogen oxides and ozone (e.g. for copper phthalocyanine, CuPc). The unique sensitivity has led to studies on the potential application of corresponding sensor structures to explore the chemical nature of the Mars atmosphere during future Mars missions.[30]

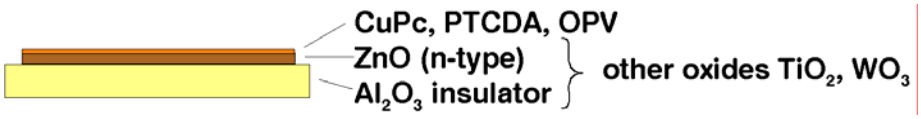

Figure 33. Thin film sensor comprising functionalized surfaces of metal oxides (ZnO, TiO_2 and WO_3). The surfaces are modified with organic molecules with the aim to increase the sensitivity of the oxide.

Metal oxide/organic film blends have been explored for their use as sensing layers for VOC detection. Needs of the industrial partners for chemical sensing include detection of waste gases from various industries and recognition of the gas contents so that undesirable chemicals could be either isolated or utilized safely.

VOC	Concentration of dominating components in waste gas, ppm[31,32,33]	vapor pressure at 22 °C, mmHg	saturated concetration in air at 750 mmHg[2)], ppm QCM tests	effective concentration at 10^{-1} Torr, ppm Conductivity tests					
water		24	20 571	2,06	acetic acid	0,030	15	42 857	4,29
iodine		0,1	1 210	0,12	propionic acid	0,013	3	10 571	1,06
ethanol		100	219 048	21,90	phenol	0,009	0,5	2 238	0,22
octanol		0,2	1 238	0,12	toluene		28	122 667	12,27
acetone		200	552 381	55,24	xylene		10	50 476	5,05
p-formaldehyde		100	142 857	14,29	ammonia		7000	5 666 667	566,67
n-butyric acid	0,060	1	4 190	0,42	p-cresol	0,002	0,2	1 029	0,10

Table 2. Properties of VOCs selected as target substances for chemical sensing.

[30] A. P. Zent et al., *Lunar and Planetary Science* **23** (2002) 1423

[31] S. Schiffman, J. Bennett and J. Raymer, *Agricultural and Forest Meteorology* **108** (2001) 213

[32] S. Willig, M. Lacorn and R. Claus, *J. Chromatography A* **1038** (2004) 11

[33] S. Rappert and R. Müller, *Waste Management* **25** (2005) 887

There was found a number of reports published, providing a comprehensive review of typical contents of waste gases from agricultural industries. Such gases may contain over 300 chemical compounds including groups of alcohols, ketones, aldehydes, fatty acids and cyclic hydrocarbons. Basing on this knowledge, a number of volatile organic compounds (VOCs) of the corresponding types were selected as target substances for the chemical sensing tests carried within the project. A typical waste gas contains a number of few dominating components and their concentrations are given in Table 2, including their saturated vapour pressures. This leads to saturated concentration values of these VOCs in air, which corresponds to the experiments carried out using the Quartz Crystal Microbalance (QCM) installation. The effective concentration during the electro-conductivity tests had substantially lower values.

The first method is based on the measurement of the frequency changes of a Quartz Crystal Microbalance (QCM) set-up ("electronic nose", operation with 8 independent QCMs). The quartz crystals (QuartzCom) were operated near the 11.5 MHz resonance frequency. The relevant VOC were mixed with synthetic air to form the testing gas samples and forwarded to the sensing chamber at a 1 liter/min stream flow. The sensor exposure time was set 10-60 s and this was followed by a 100-200 s refreshing session using pure synthetic air.

The second method utilizes electrical conductivity changes of a sensor film upon gas exposure. This procedure makes it possible to conduct sensitivity tests towards VOCs with typical effective concentrations 1-10 ppm (Table 1). The design of the experimental installation is shown schematically in Figure 34. The base pressure in the chamber was 10^{-3} Torr and opening the exposure valve let the VOC enter the sensing chamber up to a certain pressure set 10^{-1} Torr. Closing the exposure valve and opening the evacuation valve would evacuate the sensing chamber down to 10^{-3} Torr again. The external voltage applied was chosen 4V, and the electrical current J was measured. Commercial pre-amplifiers were used in the measurement circuit in order to achieve a stable registration of the electrical current down to 5.10^{-10} A values. The sensitivity K was calculated as ratio $\Delta J/J_0$, where J_0 – background current before gas exposure and ΔJ- maximum response. The time slots for the gas exposure and gas evacuation were set to appropriate values within the range from 10 s to 300 s. The following response time parameters of the sensor were monitored $\tau 1$- rise time on gas admission and $\tau 2$ – relaxation time, the time of decay to 30% of maximum response on gas evacuation.

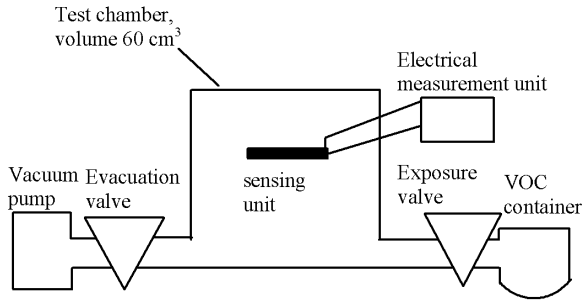

Figure 34. Scheme of the experimental installation used in the sensitivity tests by means of electrical conductivity measurements.

For the electrical sensitivity measurements, the supporting substrate was an insulating print circuit with interdigitating electrodes. Electrode spacing was 0,5 mm and total length was approximately 100 mm.

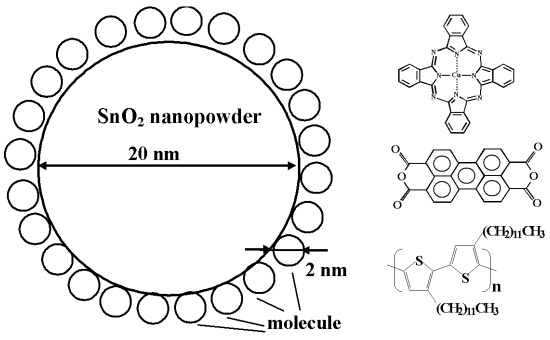

Figure 35. A scheme of a fragment of a blend sensing layer and the chemical structure of the molecular materials used in the study.

The sensing layers were prepared using drop-casting from a solution. This deposition procedure allows control of average film thickness within 1000-2000 nanometers. The surface roughness of the sensing layers was to a large extent determined by the size of the particles of the metal oxide powder, which is substantially larger than the size of the small conjugated molecules. A fragment of the blend sensing layer and the chemical structure of the molecular materials is shown schematically in Figure 35. The following metal oxide powders were used: SnO_2 nanopowder with the particle size 20 nm, TiO_2 powder with the particle size less than 5μ, and Si/SiO_2 powder with particle size 300 nm. The following conjugated organic molecules were used: Cu-phthalocyanine (CuPc), perylene tetracarboxylic acid dianhydride (PTCDA), poly (3-dodecylthiophene) (PDDT) (chemical structure is shown in Figure 35) and unsubstituted polythiophene (PTh). These metal oxide/organic film blends were tested as sensing layers for VOC detection and the overall results are presented in Table 3. The overall sensitivity results obtained were ranked as A and B type and the more detail, the results and discussion is presented in the following sections.

		Conductivity tests			QCM tests	
oxide powder	organic film	CuPc	PTCDA	PDDT	PDDT	PTh
none		B	B	B	A	A
TiO_2-5		A	A	A	B	B
SnO_2-20nm		A-	A	A-	B	B
Si/SiO_2-300nm		A	B	A	B	B

Table 3. Metal oxide/organic film blends tested as sensing layers. A and B – the overall performance of the sensor prototypes for VOC detection.

A - promising results - pronounced, selective, reversible, reproducible response towards one or a group of VOCs.

B - results are not clear for the structures alone. Supplement to increase selectivity of the A. For instance B can be used for calibration of measurements of water contents and A afterwards can quantitatively detect VOCs.

The sensitivity tests were carried out for the following sensing layers: one component PDDT, and PDDT/SnO_2 and PDDT/TiO_2 blends. The sensing response towards a series of VOCs was subjected to the analysis and the results are summarized in Table 4.

	PDDT	PDDT/	PDDT/

		SnO_2	TiO_2
water vapors	800	200	100
I_2	100	200	150
ethanol	< 0,5	< 0,5	< 0,5
p-formaldehyde	< 0,5	< 0,5	< 0,5
acetic acid	< 0,5	< 0,5	< 0,5
acetone	< 0,5	< 0,5	< 0,5
phenol	1	5	50
toluene	1,5	8	100
NH_3	< 0,5	50	400

Table 4. Sensitivity $K=\Delta J/J_0$ of the PDDT sensing layers and of its blends with metal oxide powders

PDDT containing films respond pronouncedly to I_2 vapour. Iodine is a known dopant for conjugated polymers and it is commonly used to increase conductivity in PDDT films. The exposure to water vapours results in the dominating response of the one-component PDDT films. The response to other VOCs in the series is much lower and bridged by response to water vapors. Addition of SnO_2 and TiO_2 into the sensing layers reduces the influence of water 5-10 times. Using the metal oxide powders increases the response to ammonia by about 100 times. This also increases response to phenol and toluene 5-50 times. Typical reverse relaxation time is approximately 100 s and in case of PDDT/TiO_2 it is approximately 50 s. Relaxation time after exposure to ammonia is further reduced to 20-50 s. The typical electrical response profiles towards VOCs selected are shown in Figure 36. Comparison of the response profiles of the three types of structure studied towards phenol vapor is shown in Figure 37.

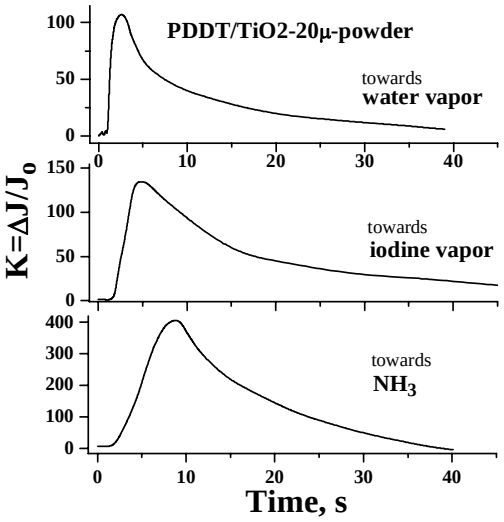

Figure 36. Electrical response of the PDDT/TiO_2 sensing layer to VOCs selected.

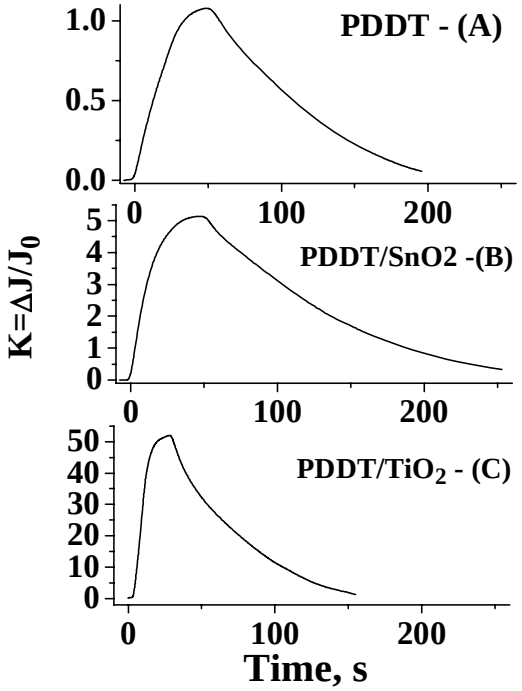

Figure 37. Electrical response of the sensing layers based on PDDT and on its blends with metal oxides towards phenol vapour.

The main conclusion on this section is that the use of SnO_2 and TiO_2 powders in the sensing layers eliminates the dominating influence of water vapour on the results. The sensing layers are promising for detection of ammonia, phenol and toluene.

For the sensitivity tests of blends of small conjugated molecules with metal oxide powders SnO_2 and on TiO_2 powders functionalised by CuPc and PTCDA molecules were chosen. The results on the sensing response towards a series of VOCs are summarized in Table 5.

	CuPc/ SnO_2	PTCDA/ SnO_2	CuPc/ TiO_2	PTCDA/ TiO_2
water	15	10	20	20
toluene	< 2	< 2	< 2	< 2
ethanol	3	20	4	25
acetone	< 2	< 2	< 2	< 2
NH3	150	20	2500	100

Table 5. Sensitivity $K=\Delta J/J_0$ of the metal oxide powders functionalized by small conjugated molecules.

A selectively high response of CuPc-containing films towards ammonia was observed. This can be explained that differently from PTCDA molecules, CuPc are electron donors relatively to the metal oxides. One may assume that CuPc form electron transfer complexes with the metal oxides, which are responsible for the high sensitivity observed. It should be noted that the

response of the blends containing TiO_2 powder is 15 times larger in average than the response of the SnO_2 containing blends. On the other hand, the oxide powders functionalised by PTCDA show a selective response to ethanol vapour. Typical values of the reverse relaxation time are 15-20 s for the sensing layers studied. The typical electrical response profiles of structures studied are shown in Figure 38.

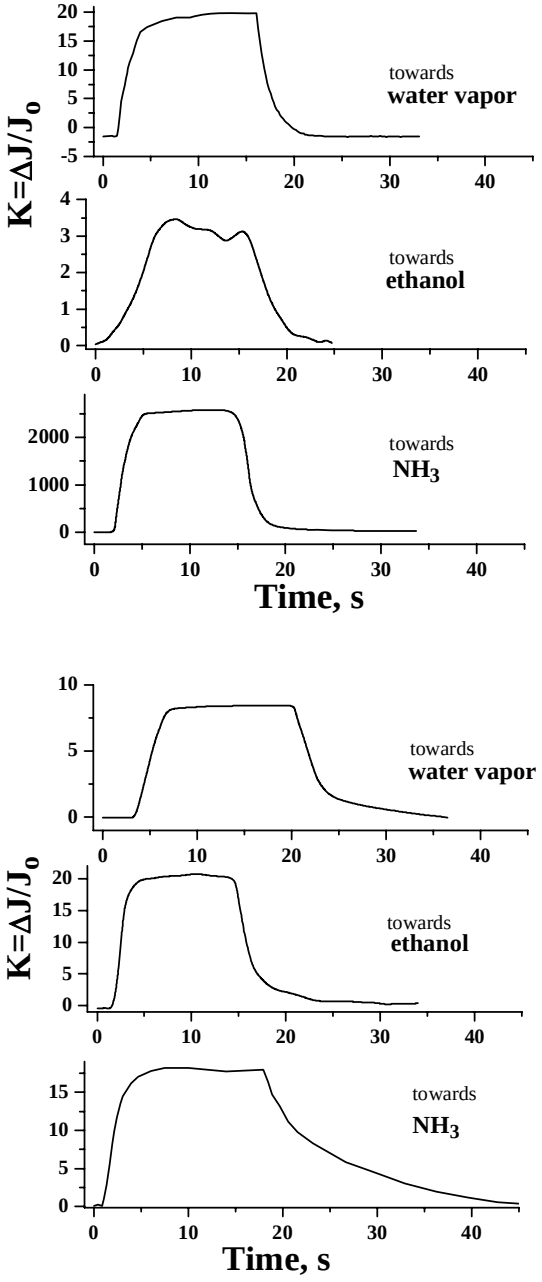

Figure 38. Electrical response profiles of the CuPc/TiO_2 film (top) and of the PTCDA/TiO_2 film (below) towards VOCs selected.

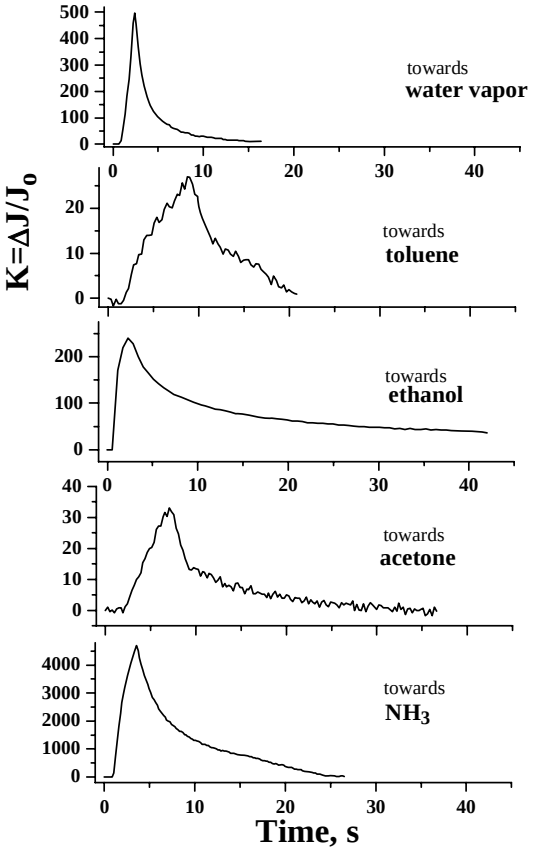

Figure 39. Electrical response of the CuPc/Si/300nmSiO_2 to common volatile compounds

The CuPc/metal oxide blend films show a highly pronounced response to ammonia. These structures differ from the ones based on PTCDA because they are known to have electron transfer between the components. The PTCDA-containing films studied showed a low background response to water and to ammonia vapour while they have an enhanced response to ethanol.

The sensor properties of Si-SiO_2 powder functionalized with CuPc, PDDT and PTCDA towards various VOCs are summarized in Table 6.

	Si-SiO_2	CuPc/ Si-SiO_2	PDDT/ Si-SiO_2	PTCDA/ Si-SiO_2
water	20	500	1000	50
toluene	10	30	120	10
ethanol	150	250	70	10
acetone	< 1	30	30	< 1
NH_3	30	4700	4500	20

Table 6. Sensitivity $K=\Delta J/J_0$ of the Si-SiO_2 powder functionalized by conjugated organic molecules

CuPc and PDDT - containing films show a selectively high response of towards ammonia. As it was discussed in the previous section, there may be suggested that formation of the electron transfer complexes within these blends may account for this selective sensitivity. According to the results in the table 5, the silicon oxide powders functionalised by the electron donating organic molecules can also be used for detection of toluene, ethanol and acetone. The PTCDA-containig structures showed an overall low sensitivity during the tests carried out. Typical values of the reverse relaxation time are 5-10 s for the sensing layers studied. The typical electrical response profiles of structures studied are shown in Figure 39. Silicon oxide powders functionalised by the electron donating organic molecules such as CuPc and PDDT show a highly pronounced response to ammonia, they can also be used for detection of toluene, ethanol and acetone.

	PDDT	PDDT/ SnO_2	PTh	uncovered, reference
room air	40	30	60	5
waste gas *force	50	40	100	10
water vapor	55	70	250	12
ethanol	125	xxx	190	30
octanol	90	20	105	10
p-formaldehyde	60	xxx	90	10
acetic acid	30	xxx	100	10
propionic-acid	450	xxx	150	5
phenol	154	xxx	110	25
toluene	2100	xxx	100	20

Table 7. Sensitivity measured as a change of the QCM frequency in Hz of the PDDT, PDDT/SnO_2 and PTh sensing layers

Results of the sensitivity tests with QCMs with PDDT, PTh and PDDT blended with metal oxide powder are summarized in Table 7. The response of the mixed PDDT/SnO_2 film was often unstable. This may be attributed to the mechanical changes in the film structure containing a few nm large metal oxide particles caused by the oscillations of the QCM. Both PDDT and PTh show a response towards the VOCs tested, which is much more pronounced than the response of the reference quartz crystal. The response to water vapour plays particularly a minor role in case of the PDDT sensing film (Figure 40).

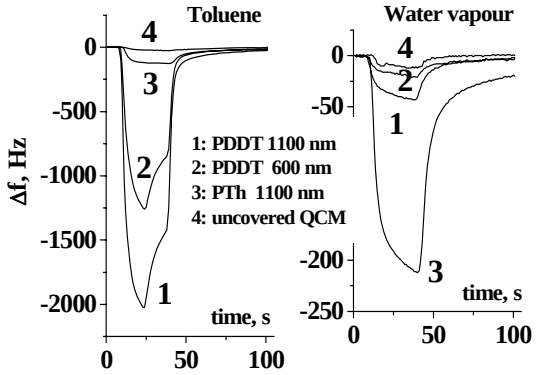

Figure 40. QCM response of the PDDT and PTh sensors towards water vapour and toluene

7 Impact on industry

Apart one independent non-profit institution (FORCE Technology), four SMEs belong to the consortium of the NanoChemSens project. PBI-Dansensor A/S is a worldwide supplier of high-quality gas instrumentation equipment for on-line and off-line process control and laboratories. The company develops, manufactures and markets gas analysers, gas mixers, automated gas purging systems, leak detectors and permeability testers. The portfolio of VEGATEC includes, among various micro- and nanotechnological technologies, gas panel and gas handling instrumentation. Bernt Messtechnik is a devoloper of complete metrological equipments and installations, mainly for gas analysis. Danish Micro Engineering A/S, being one of the oldest manufacturers of AFM, STM, and SNOM equipment on the market, provides software, microelectronics, and SPM microscopes. In conclusion, the industrial partners have minor to a medium-level research capacities in the nanotechnological area.

The industrial partners have been fully involved at all management activities of project, in many workpackages, including the last project year which was supervised by PBI. Specifically, activitive cooperations between the research teams of the universities and the industrial partners started during the second year. This concerns the use of functional organic molecules, deposited over quartz microbalance sensors, which are studied in a cooperative effort (RUC/FOR). The main focus was the possible use of arrays of QMB sensors for odor recognition in animal farms. The deposition of WO_3 nanorods over SiO_2/Si and a possibly improved or controlled growth by ion implantation techniques is a subject of interest for VEG, besides the test of such structures. A closer cooperation has been achieved between UDESAM and VEG on WO_3-based film and nanorod structures. Specifically, experiments have been performed to grow WO_3 nanorods on oxidized silica wafer and study the role of potassium promotors. BER has provided know-how to UDUS in the context of the development of a eight-sensor electronics in the last project year. PBI is a partner with a variety of sensor test facilities, providing also interfaces/electronics parts, as well as information about the needs of endusers. The applicability of atomic force microscopy and scanning tunneling microscopy to study sensor surfaces has been studied by DME in cooperation with UDUS and other partners. More information is available in the Periodic Activity Report of 05.06.07.

8 Project summary

The major focus of the NanoChemSens project was to prepare and characterise properties of the model structures with respect to their adsorption and sensing properties and to test some of the structures with respect to “real world” performance in typical sensor applications. In connection with the microscopic and spectroscopic data, potential routes towards sensor development for nanostructured sensors should be derived. The project objectives concern heterojunctions, metal-oxide-metal tunnel junctions, pn junctions, epitaxial layers, nanorod assemblies, and functional organic molecules and ionophores for mass-sensitive devices; emphasis was put on a few selected metal oxides and metals..

The major achievements for the different model systems are:

- For Pt/TiO_2 heterojunctions, we succeeded to determine the current-voltage curves of a single Pt particle with a diameter of 8 nm, deposited on a clean titanium oxide surface; the shape of nonlinear *I*-*V*-curve depends on the oxygen partial pressure.
- For clean TiO_2 surfaces a number of surface reactions, relevant in the context of cross-sensitivity of oxide sensors towards humidity, could be identified by scanning tunneling microscopy. Concerning the doping of clean surfaces, the main reactions of molybdenium surface additives have been investigated.
- The structural characterisation of ultrathin TiO_x films on single crystal platinum surfaces has been completed; doping experiments with nanosized Au clusters were performed that indicates a route towards narrow size distributions of such additives.
- Prototypes of WO_3 thin film sensors have been developed and tested; a multisensor electronics was constructed for this sensor device. Assemblies of WO_3 nanorods were prepared and their sensing properties were determined. Based on these studies, well-defined percolation-type sensors seem to be accessible.
- A heterojunction based on zinc oxide and copper oxide have been synthesized in ultrahigh-vacuum; first electrical measurements were performed.
- Metal oxide/organic film blends have been explored for their use as sensing layers for detection of volatile organic compounds. TiO_2 surfaces have been modified with phendione; this compound may provide sensitivity towards ethylene via a guest-host interaction.

Appendix 1 Using and dissemination of knowledge

Overview table					
Planned/actual Dates	**Type**	**Type of audience**	**Countries addressed**	**Size of audience**	**Partner responsible /involved**
2004	*Universities´ web-sites*	*General public*	*EU*		*Participating universities*
2004 - 2007	*Workshops, Conferences*	*Research*	*EU, International*	*Typ. 50-200*	
2004 - 2007	*Publications*	*Research*	*EU, International*		
2004 - 2007	*Project web-site*		*EU, International*		

Universities´ web-sites

In 2004 all participating universities announced the NanoChemSens project through their web pages to the general public, typically to an interested local audience of the different cities. The impact of such notifications is unquantifiable; however, in many cases partners have been asked to participate in local or national questionnaires on nanotechnological-oriented projects.

Workshops, Conferences and Publications

C.L. Pang, O. Bikondoa, D.S. Humphrey, A.C. Papageorgiou, G. Cabailh, R. Ithnin, Q. Chen, C.A. Muryn, H. Onishi, G. Thornton, Nanotechnology 2006, 17, 5397

A.J. Limb, O. Bikondoa, C.A. Muryn, G. Thornton, Angewandte 2007, 46, 549

G. Teobaldi, W.A. Hofer, O. Bikondoa, C.L. Pang, G. Cabailh, G. Thornton, Chem. Phys. Lett. 2007, 437, 73

A.C. Papageorgiou, G. Cabailh, Q. Chen, A. Resta, E. Lundgren, J.N. Andersen, G. Thornton, Submitted to J. Phys. Chem. C

A.C. Papageorgiou, C.L. Pang, Q. Chen, G. Thornton, Manuscript in preparation

A.C. Papageorgiou, C.L. Pang, D. Humphrey, G. Cabailh, G. Thornton, Manuscript in preparation

G. Thornton, “Templating tethering sites on an oxide surface” (Invited), 2006 Symposium on Surface Physics, Shizukuishi, Japan, 11-13 January 2006

G. Thornton, “Structure and reactivity of TiO_2(110)”, (Invited), Molecular Modelling Meeting 2006, University of Limpopo, South Africa, 4-6 April 2006

G. Thornton, “How single atom defects can influence a photocatalyst “, (Invited), Microscience 2006, London, United Kingdom, 27-29 June 2006

G. Thornton, “Water chemistry on TiO_2(110)”, (Invited), American Chemical Society Meeting, San Francisco, California, 10-14 September 2006

G. Thornton, “Formation and reaction of TiO_x nanostructures”, (Invited), Spanish Vacuum Society Workshop on Nanostructures, Avila, Spain 24-27 September 2006

G. Thornton, Keynote Single Molecule water chemistry on TiO_2(110), (Invited), New Zealand Institute of Chemistry 2006, Rotorua, New Zealand, 2-6 December 2006

G. Thornton, Imaging and manipulating oxide surfaces, (Invited), Symposium on Surface and Nano Science, Appi, Japan, 24-26 January 2007

G. Thornton, Single reactions on a model photocatalyst, (Invited), IFCAM Workshop on Surface and Interface Science, Sendai, Japan, 26-27 January 2007

A. Papageorgiou, "Rutile TiO_2 (110) on the ultra-thin limit", Surface Science Summer School, The University of Nottingham, UK, 21-26 August 2005

A. Papageorgiou, "High resolution photoemission characterisation of the growth and reactivity of thin film titanium oxides", Annual NanoChemSens meeting, Brixen, Italy, 20-21 January 2006

A. Papageorgiou, "Structure and reactivity of Cr-doped TiO_2(110) surface", Annual NanoChemSens meeting, Brixen, Italy, February 2007

G. Granozzi : TiOx Nanostructures on Pt(111) and Pt(110) Substrates: a Combined LEED, Photoemission, STM and Theoretical Investigation (invited), International Workshop on Oxide surfaces (IWOX V, Lake Tahoe, USA, 7-12 january 2007).

G. Granozzi (invited), TiO_x nanostructures on Pt(111) and Pt(110) substrates: a combined experimental and theoretical investigation, COST action D41/ Inorganic oxide surfaces and interfaces (Vienna/Austria, November 2-4, 2006)

Granozzi, Nanolayers of TiO_x on Pt substrates: a combined LEED, Photoemission, STM and theoretical investigation, Workshop on the Reactivity and Stability of Surfaces and Nano Particles at Elevated Temperatures (Kloster Irsee , Germany, 27-30 september 2006).

G. Granozzi, Preparation and structure of oxide nanostructures on metal single crystals, NIS Colloquia Nanostructured Oxide Surfaces, Torino February, 17-18 2005

G. Granozzi: Preparation, structural characterization and reactivity of oxide based surface nanostructures, Workshop: In situ atomic scale characterization of surfaces under high pressures: recent advances in experiment and theory, CECAM Lyon, November 4-6 2004

G. Granozzi: Preparation and structure of oxide nanostructures on metal single crystals X-th Symposium on Surface Physics, July 10-15, 2005, Prague, Czech Republic.

G. Granozzi: Preparation and characterization of well ordered TiO_x nanostructures on Pt(111). International Workshop WS17 on TiO2, July 24-27,2005, Avila, Spain

F. Sedona, F. X. Llabrés i Xamena, M. Eusebio, G. A. Rizzi, G. Granozzi, D. Ostermann and K. Schierbaum, Growth and structure of ultrathin films of TiO_x on Pt(111), The Fourth International Workshop on Oxide Surfaces (IWOX-4), Torino, Aussois, January 4-8, 2005

T. Orzali, M. Sambi and G. Granozzi, Surface structure of ultrathin films of TiO_x on Pt(110), The Fourth International Workshop on Oxide Surfaces (IWOX-4), Torino, Aussois,January 4-8, 2005

G. Granozzi, M. Sambi and G.A. Rizzi, Surface supported oxide nanostructures as innovative functional materials and model systems for supported catalysts (invited) Syntheses and Methodologies in Inorganic Chemistry, (SAMIC 2004), Trends in Nanoscience, 5-7 December 2004, Bressanone (BZ), "Phendione on TiO2", MAX-lab Activity Report 2005/06

M. Kölbach and K.D. Schierbaum, STM and point contact formation of Pt nanosized particles on TiO_2(110), manuscript in preparation.

A. S. Komolov and P.J. Møller, Appl. Surf. Sci., 2005, Vol. 244, p. 573-577.

A. S. Komolov, P.J. Møller, Y. G. Aliaev, E. F. Lazneva, S. Akhremtchik, J. Mortensen, F. S. Kamounah and K. Schaumburg, J. Molec. Spectr., 2005, Vol. 744-747, p.145-149.

A. S. Komolov, P. J. Møller, J. Mortensen, S. A. Komolov and E. F. Lazneva, Surf. Sci., 2005, Vol. 586, p. 129-136.

Komolov A. S., Akhremtchik S., Møller P., J. Phys. Low-Dim. Struct., 2006, Vol. 2, p. 58-63.

Komolov A. S., Møller P. J., Mortensen J., Komolov S. A. and Lazneva E. F., Appl. Surf. Sci., 2007, accepted

A.S. Komolov and P.J. Møller, Unoccupied electronic band structure of conjugated molecular films interfacing polycrystalline gold surface, ICSFS-12 conference, Hamamatsu, Japan, June 21-25, 2004

A.S. Komolov, P.J. Møller, Y. G. Aliaev, E.F. Lazneva, S. Akhremtchik, F. S. Kamounah and K. Schaumburg, Organic-organic interfaces and unoccupied electronic states of thin films of perylene and naphthalene derivatives, 27th European Congress on Molecular Spectroscopy, Krakow, Poland, September 5-10, 2004

Komolov A. S., Møller P. J., Mortensen J., Komolov S. A. and Lazneva E. F., Electronic properties of ultra thin conjugated organic layers on the TiO_2 (110) surface. XIII international conference on Solid films and surfaces, San Carlos de Bariloche, Argentina, 6-10 Nov 2006, p. Th-Gro 194.

Pengchao Si, Alexei Komolov, Jens Denborg, John Mortensen, Preben Juul Møller, Polythiophene coatings on quartz crystal oscillators for detection of volatile organic compounds in mixtures, International Symposium on Olfaction and Electronic Nose, St. Petersburg, Russia, 3-5 May, 2007, accepted

M. Gillet, R. Delamare, E. Gillet, Growth,structure and electrical conduction of WO_3 nanorods, 13th Internatinal Conference on Solid films and Surfaces (ICSFS 13);6-10 november 2006, Bariloche, Argentina

A. Labidi, E. Gillet, R. Delamare, M. Maaref, K. Aguir, Sensors and Actuators B 122 (2006) 380.

E.Gillet, K. Masek, D. Lollman, M. Gillet, Evolution of the oxidation states at the WO_3 thin film surface during annealing in gases, Joint Vacuum Conference(JVC 11):25-28 september 2006. (Prague)- Czech Republic.

R. Delamare, M. Gillet, Ph. Gaino, E. Gillet, Structure and electrical properties of tungsten oxide nanorods epitaxially organised on a mca substrate, Oral presentation in: International Conference on Nano-structures Self-Assembling:2-6 july 2006. (Aix-en-Provence) France.

Ph. Gaino, M. Gillet, R. Delamare, E. Gillet, Local modification of electrical properties of tungsten oxide nanorods using Conductive Atomic Force Microscopy, accepted for publication in Surface Science.

R.Boulmani, M. Bendahan, C. Lambert-Mauriat, M. Gillet, K. Aguir, Local modification of electrical properties of tungsten oxide nanorods using Conductive Atomic Force Microscopy, accepted for publication in:Sensors and Actuators B.

M. Gillet, R. Delamare, E. Gillet, Stucture and electrical conduction of WO_3 nanorods epitaxially grown on mica, accepted for publication in :The European Physical Journal.

Project web-site

A project's web page has been available at: http://www.nanochemsens.uni-duesseldorf.de during the reporting periods (01.03.2004 – 28.02.2007) of the NanoChemSens project.